BMC Genomics

RESEARCH

Open Access

An updated and spatially validated somatic single-cell atlas of *Hydractinia symbiolongicarpus*

Jingwei Song[1,2,3†], Danielle de Jong[1,2†], Justin Waletich[1,2], Andreas D. Baxevanis[4] and Christine E. Schnitzler[1,2*]

Abstract

Single-cell RNA sequencing (scRNA-seq) has revolutionized transcriptomic research, enabling the creation of detailed tissue, organ, and species-level atlases for model organisms. In *Hydractinia*, a cnidarian model for stem cell and regeneration studies, recent atlases have revealed key insights into cell types and developmental processes. However, these atlases remain limited in cell numbers and transcriptomic depth and cell type assignments were largely made in silico. Here, we present an updated *Hydractinia* single-cell atlas by integrating new datasets from fixed cells with previously published live-cell data. This expanded atlas captures over 47,000 cells from feeding polyps and stolon tissue, recovering and refining major somatic cell lineages including cnidocytes, neurons, gland cells, epithelial cells, and stem cells (i-cells), as well as identifying a novel population of putative immune cells. We investigated the spatial expression patterns of selected marker genes and validated all major cell types and several cell states. Our analyses uncovered a previously undescribed neural subtype, two spatially distinct gland cell populations, a stolon-specific cell type, and a putative immune cell cluster. Additionally, we recovered and explored a complete *Hydractinia* cnidocyte trajectory with two distinct endpoints, supported by spatial marker gene expression that reflects the developmental progression of cnidoblasts as they mature and migrate towards the tentacles. Subclustering of somatic i-cells revealed putative progenitor states and a potential population of true stem cells. Together, this atlas significantly advances our understanding of *Hydractinia* cellular diversity and dynamics, allowing us to generate new hypotheses and provide a valuable resource for the cnidarian research community and beyond.

Keywords cnidarian, hydrozoan, *Hydractinia symbiolongicarpus*, single-cell atlas, neuron, cnidocyte, i-cells, epithelial cells, immune cells, gland cells

†Jingwei Song and Danielle de Jong contributed equally to this work.

*Correspondence:
Christine E. Schnitzler
christine.schnitzler@whitney.ufl.edu
[1]Whitney Laboratory for Marine Bioscience, University of Florida, 9505 Ocean Shore Blvd, St. Augustine, FL 32080, USA
[2]Department of Biology, University of Florida, Gainesville, FL 32611, USA
[3]Department of Fisheries, Wildlife, and Conservation Sciences, Coastal Oregon Marine Experimental Station (COMES), Hatfield Marine Science Center, Oregon State University, Newport, OR 97365, USA
[4]Division of Intramural Research, National Human Genome Research Institute, National Institutes of Health, Bethesda, MD 20892, USA

Introduction

Hydractinia is a fascinating genus of colonial marine hydrozoans that has captivated scientists since the late 19th century, largely because of its remarkable stem cell biology and extraordinary regenerative abilities, allowing the organism to regrow any part of its body at any time [1]. These organisms have experienced a resurgence of interest in the molecular era owing to their suitability for genetic manipulation, microscopy, and molecular studies [2, 3]. Advances in genomics, including the sequencing of new genomes, transcriptomes, and the development of transgenic lines, have positioned *Hydractinia* as an emerging model organism for studying fundamental biological processes including regeneration and stem cell biology.

The *Hydractinia* colony consists of multiple polyp types connected via a basal mat encompassing a network of endodermal gastrovascular canals called stolons, located between two ectodermal epithelial layers. The two most common polyp types in cultured animals are gastrozooids (feeding polyps) (see Fig. 1a) and gonozooids (sexual polyps). In nature, defensive polyps are also present (dactylozooids and tentaculozooids). The feeding polyp has ectodermal (epidermal) and endodermal (gastrodermal) layers that are separated by an acellular mesoglea; it also contains several specialized cell types such as cnidocytes, neurons, gland cells and epithelial cells (Fig. 1b). *Hydractinia* also contains a population of stem cells called interstitial cells (i-cells). These i-cells have traditionally been characterized by their size, morphology, location, and staining properties [4–6] and, more recently, through the expression of marker genes such as *Piwi1* and *Vasa* [7, 8]. However, it remains unclear whether the cell populations identified using different methods (e.g., morphology, staining, or marker gene expression) represent the same cellular population or if these methods also include progenitor populations. *In situ* hybridization (ISH) studies of various stem cell marker genes have generally confirmed the locations of i-cells in the colony but have revealed discrepancies in the number and morphology of cells stained, suggesting potential heterogeneity within these populations [9, 10]. Single-cell RNA sequencing (scRNA-seq) holds great promise for resolving these questions, as it allows for the bioinformatic clustering of cells with overlapping transcriptomic profiles and the identification of cell-type marker genes, providing insights into cellular diversity, cell states, and function.

scRNA-seq has revolutionized genomics by enabling researchers to analyze transcriptomes of individual cells [11]. Initially applied to mammalian models, this technology has since been utilized to study a wide range of organisms, including various cnidarian species [12–17]. Two previous studies using two different approaches generated single-cell atlases for *Hydractinia symbiolongicarpus* (hereafter, *'Hydractinia'*, unless specified otherwise), and provided many new biological insights. One study combined cells from feeding polyps, sexual polyps, and stolons, identifying a somatic i-cell cluster, and a germ i-cell cluster connected to a complete trajectory of spermatogenesis [18], while the second study separately profiled stolons and two polyp types to investigate the distribution of cell types across the colony [19]. These efforts also faced limitations such as being based on a relatively low number of cells ($n = 8{,}888$), leading to several small cell clusters that were difficult to characterize [18] or providing limited gene coverage per cell (median genes per cell < 100) resulting in unresolved and overlapping clusters that were not spatially validated [19]. These atlases can be significantly improved by increasing both the number of cells analyzed and the depth of gene coverage, resulting in a more comprehensive and higher-resolution single-cell atlas followed by spatial validation of cell clusters. This, in turn, will provide deeper biological insights, facilitate further hypothesis generation, and serve as a valuable resource for future studies.

Previously, we identified two distinct subpopulations of i-cells in our original *Hydractinia* single-cell atlas: one that gives rise to germ cells and another that differentiates into either cnidoblasts (stinging cell progenitors) or neurons [18]. However, the low number of i-cells captured in that study limited further exploration of these i-cell subpopulations. This new study aims to overcome the limitations by providing an improved, comprehensive single-cell atlas that encompasses all somatic cell lineages in *H. symbiolongicarpus*.

Here, we present an updated *Hydractinia* single-cell atlas containing over 47,000 cells derived primarily from feeding polyp and stolon tissue, consisting of 19 cell-type and cell-state clusters (Fig. 1c). We have validated all major cell types in these clusters, as well as select cell differentiation states, using fluorescent *in situ* hybridization (FISH) and hybridization chain reaction-FISH (HCR-FISH) methodologies. This approach has revealed several major findings, including a previously undescribed neural subtype, two spatially separate gland cell populations resembling those found in *Hydra*, a stolon-specific cell type, and a putative immune cell cluster. In addition, we provide the first complete cnidocyte trajectory for *Hydractinia* and have validated expression of several markers along this trajectory. Finally, we subclustered the somatic i-cell cluster and were able to identify and assign putative cell states to i-cell subclusters. This subclustering analysis revealed a potential population of true i-cells as well as early progenitor populations (Fig. 7). We have identified multiple cell-type and cell-state specific markers that can be used to investigate biological phenomena such as regeneration and cellular differentiation. These markers also reveal previously unrecognized

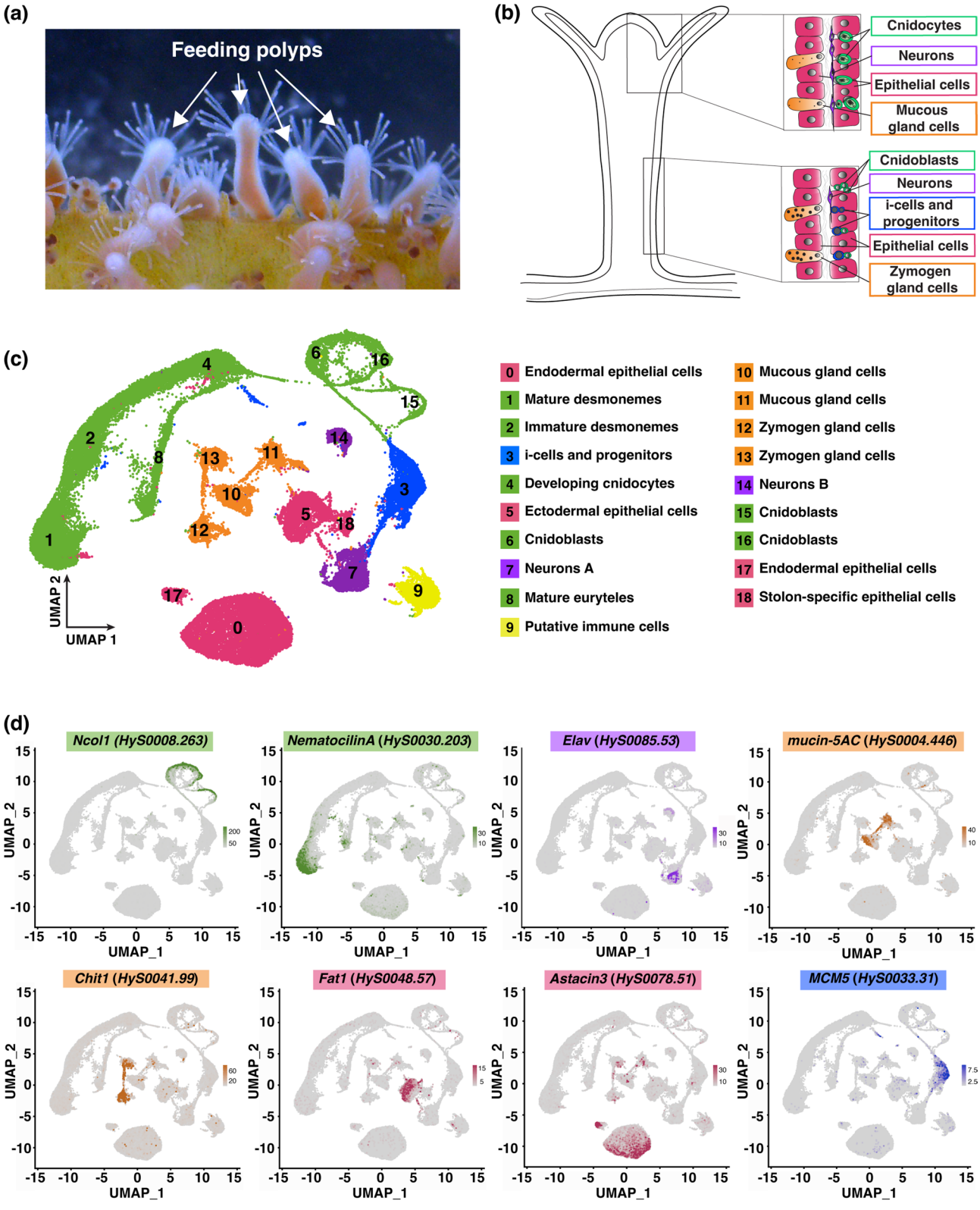

Fig. 1 (See legend on next page.)

(See figure on previous page.)

Fig. 1 Overview of *Hydractinia* feeding polyp cell types and the updated single-cell atlas. **a** Photograph of a *Hydractinia* colony, with feeding polyps indicated. **b** Schematic of a feeding polyp, showing the major cell types present in the two cell layers (gastrodermis and epidermis), separated by the mesoglea. There are some oral-aboral differences in cell types and the hypostome/tentacles of the feeding polyp contains some different cell types to the lower polyp body. **c** Two-dimensional Uniform Manifold Approximation and Projection (UMAP) representation of the updated *Hydractinia* single-cell atlas (47,901 cells), with major cell states and cell types labeled. **d** UMAP expression of specific genes that characterize the different cell states/cell types. Colors are consistent between all panels: green = cnidoblasts and cnidocytes, purple = neurons, orange = mucous and zymogen gland cells, maroon = ectodermal and endodermal epithelial cells, blue = i-cells and progenitors, and yellow = putative immune cells

transcriptional diversity within specific cell types that may underlie functional differences within the animal, allowing us to gain a deeper understanding of the genetic mechanisms governing the differentiation of progenitor cells into specific cell types. The regulatory sequences of these markers could be used to drive fluorescent reporters in a cell type- or cell state-specific manner.

Results and discussion

We initially processed raw sequencing reads through Cell Ranger v7 to compare cell level metrics among the libraries prepared from different methods (Supplementary Table S1). Two previously generated live cell libraries from feeding polyp, sexual polyp, and stolon tissue had the highest median genes per cell (792), fraction reads in cells (83.3%), and sequencing saturation (92.6%) [18]. Our new data were derived from feeding polyp and stolon tissue only, solely using fixed samples (methanol and ACME). The methanol-fixed libraries had the highest mean total genes detected (17,786) but the lowest fraction of reads in cells (33%). Methanol is known to cause mRNA leakage from the cytoplasm [20], which could have contributed to the low percentage reads in cells and low mean reads per cell (57,122). The ACME-fixed libraries had the highest mean reads per cell (162,991) but the lowest mean percentage of reads confidently mapped to the genome (41%), suggesting a potential RNA degradation worse than that observed using the methanol-fixed samples (Supplementary Table S1). Regardless of cell preparation methods (live or fixed), our median genes per cell (~ 600 – 800) was substantially higher than what was observed in a previous *Hydractinia* atlas (< 100) [19]. Overall, live cells had the best summary statistics from Cell Ranger. Although some of the summary statistics of both fixation methods were inferior to that of the live cells, both yielded data sufficient for data integration with the live cell dataset (below) and all cell clusters were recovered by each sample type (Supplementary Fig. S1a).

In this study, we focused on the somatic cell types of *Hydractinia* and excluded germ cells. For the previously generated live-cell dataset, we first removed all sperm progenitors, mature sperm cells, and sperm doublets ($n = 4{,}865$), which together comprised about 50% of that dataset. After quality control (QC) of each fixed cell dataset and subsequent integration of all three datasets, we obtained a final merged dataset comprised of 47,901 cells (26,247 methanol-fixed, 17,631 ACME-fixed, and 4,023 live cells). By combining known cell-type specific genes with the results of a literature search for the top differentially expressed genes, we identified five major somatic cell lineages in *Hydractinia*: cnidocytes, neurons, gland cells, epithelial cells, and i-cells/progenitors (Fig. 1c-d; Supplementary Fig. S1b-c). We also identified a cluster that could not be readily assigned to any known cell type but which we have putatively labeled as immune cells, a designation that is discussed below. A list of diagnostic genes used to annotate the clusters is provided in Supplementary Table S2, and their expression patterns within the single-cell atlas is shown as Supplementary Fig. S2b-c. From this point forward, major cell lineages will be presented and discussed individually.

Cnidocytes and cnidogenesis

One of the most prominent features of the new single-cell atlas is the developmental trajectory of cnidocytes (cnidogenesis; Fig. 2a), which was only partially recovered from the two previous atlases of *Hydractinia*. Neither of the two previous atlases had a complete trajectory joining i-cells and cnidocytes [18, 19]. In our atlas, cnidoblasts (C6, C15, C16) and developing cnidocytes (C4) were intermediary between the i-cell and progenitor cluster (C3) and the mature cnidocytes (C1, C2, C8) (Supplementary Fig. S1b). Both CytoTRACE and pseudotime analyses confirmed the maturation of cnidocytes along this trajectory and the single-cell atlas, CytoTRACE, and pseudotime analyses all revealed a single cnidogenesis pathway that splits into two terminal endpoints (Fig. 2a, '1' and '2'). A heatmap generated using a combination of known cnidogenesis genes and novel markers highlighted a subset of genes expressed along this trajectory (Fig. 2b). Spatial expression analysis shows that early-cnidogenesis genes such as *Txd12* (*HyS0042.111*, Fig. 2c-c‴) and *Fkbp14* (*HyS0020.22*, Supplementary Fig. S3a-a‴), as well as mid-cnidogenesis genes such as *Ncol1* (*HyS0008.263*, Fig. 2d-d‴) and *Dkk3* (*HyS0056.50*, Supplementary Fig. S3b-b‴), are all expressed in the lower half of the feeding polyp body column, a region known to harbor i-cells and cnidoblasts (Fig. 1b) [10, 21].

Mid-to-late stage cnidogenesis genes such as *Laminin* (*HyS0032.220*, Fig. 2e-e‴) and *Arstnd2-like* (*HyS0042.80*, Supplementary Fig. S2b-c; Supplementary Fig. S3c-c‴) showed expression in cells in not only the lower half of the body column, but also in cells extending towards the upper half. These genes were often detected in cells

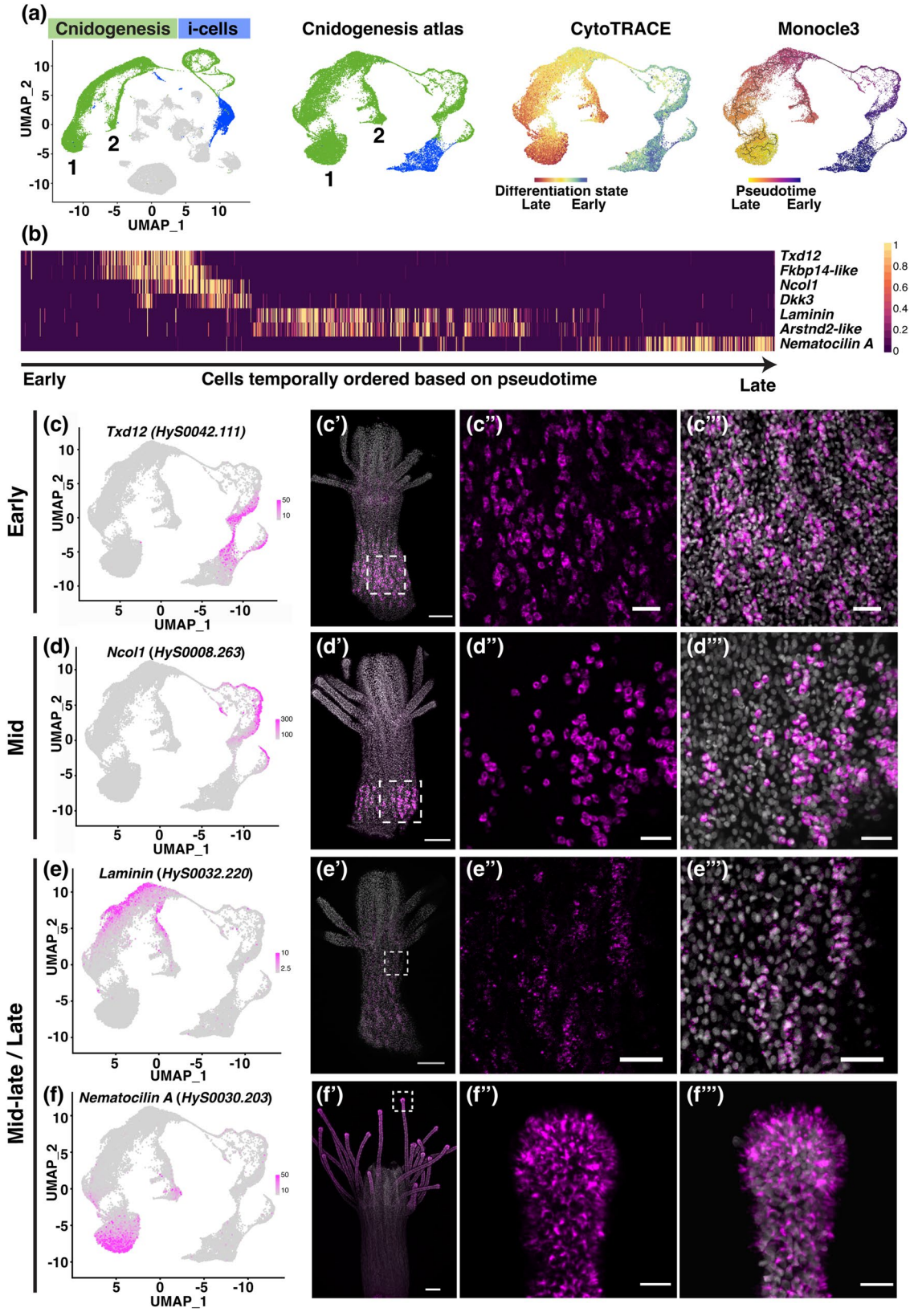

Fig. 2 (See legend on next page.)

(See figure on previous page.)

Fig. 2 Cnidogenesis trajectory from i-cell/progenitors to mature cnidocytes. **a** Single-cell atlas showing cells involved in cnidogenesis (green) originating from a single cluster of i-cell/progenitors (blue). These clusters were selected and subjected to reclustering to form the cnidogenesis atlas, upon which both CytoTRACE and Monocle3 analyses were performed. CytoTRACE shows the differentiation state from early (blue/green) to late (orange/red), while Monocle3 provides a pseudotime analysis from early (purple) to late (yellow). The two endpoints in the single-cell atlas and cnidogenesis atlas are labeled as '1' and '2', representing transcriptionally distinct, fully differentiated cnidocytes. **b** Heatmap depicting the normalized expression of seven selected genes. Each column represents an individual cell that was ordered based on their pseudotime values from the lowest (earliest) to the highest (latest). **c**-f''' Left-most column shows the expression of a particular gene in the cnidogenesis atlas, while panels to the right show expression of that gene in an adult feeding polyp. Dotted white boxes in (c'), (d'), (e'), and (f') indicate the regions shown at higher magnification in (c")-(c'''), (d")-(d'''), (e")-(e''') and (f")-(f''') respectively. Gene expression is shown in magenta, and nuclei are shown in grey. *Txd12* (*HyS0042.111*) is a marker of early cnidogenesis (c)-(c"), *Ncol1* (*HyS0008.263*) is a marker of mid-cnidogenesis (**d**)-(d'''), while *Laminin* (*HyS0032.220*) and *Nematocilin A* (*HyS0030.203*) are markers of mid-to-late and late cnidogenesis (**e**)-(f'''). Gene expression was visualized via HCR-FISH for *Txd12* (*HyS0042.111*), *Ncol1* (*HyS0008.263*) and *Laminin* (*HyS0032.220*), while FISH was used to visualize *Nematocilin A* (*HyS0030.203*) expression. Scale bars: 100 µm in (c'), (d'), (e') and (f'); 20 µm in all other panels

with distinguishable cnidocyte capsules, supporting the idea that cnidocytes migrate as they mature [18, 22, 23]. A late-stage/mature cnidogenesis marker, *Nematocilin A* (*HyS0030.203*, Fig. 1d, Supplementary Fig. S2b-c) [24] was present at both endpoints of the trajectory (C1/C8, Fig. 1c) and was expressed exclusively in the tentacles (Fig. 2f-f''') [18], confirming the two end branches of this trajectory (C1 and C8) contain mature cnidocytes. There are two major cnidocyte types known in adult *Hydractinia* feeding polyps: desmonemes and euryteles. Desmonemes are smaller than euryteles, and the morphology of their cnidocyst capsules also differs between the two types [25–27]. Given that desmonemes constitute ~ 75% of tentacle cnidocytes in *Hydractinia* and euryteles constitute the remaining ~ 25% [21] and considering that C1 is larger than C8 and expressed *Hydra* desmoneme markers (Supplementary Table S2), we hypothesized that C1 corresponded to desmonemes and C8 to euryteles. To test this hypothesis, we designed HCR-FISH probes for two new marker genes expressed specifically in each of the two clusters: *HyS0002.425* (at the tip of C1, Supplementary Fig. S3d) and *HyS0027.82* (at the tip of C8, Supplementary Fig. S3e). *HyS0002.425* was expressed in cells throughout the tentacles and only sparsely in the body column (Supplementary Fig. S3d'-d'''). *HyS0027.82* was expressed in cells concentrated at the tentacle tips, as well as in cells sparsely distributed throughout the tentacles (Supplementary Fig. S3e'-e'''). A double HCR-FISH experiment showed that the two populations of cnidocytes were non-overlapping (Supplementary Fig. S3d''', S3f-f'). However, the dense packing of cnidocytes in the tentacles made size comparisons difficult, and it was not possible to confidently measure differences in capsule size of cells expressing either marker. Similar double HCR-FISH images are shown in Fig. 2 of [28], where we discuss how single-cell transcriptomics is informing our understanding of cnidarian sensory biology. In that figure, a magnified image of the mid-tentacle region of a feeding polyp shows that the same two markers are non-overlapping in this region and includes a panel showing differential interference contrast (DIC) illumination highlighting cnidocyst structures. Overall, the results supported our hypothesis that the larger end branch represents desmonemes (C1) and the smaller branch represents euryteles (C8).

Comparison of our cnidogenesis trajectory with those of other cnidarians revealed a close resemblance to that of *Hydra* [29], where mature cnidocytes form distinct clusters based on their type. This contrasts with findings from *Nematostella vectensis*, where the cnidocyte trajectory derives from a single pool of progenitors that splits into multiple differentiation pathways corresponding to the different cnidocyte types before the trajectory converges into a single cluster [16, 30]. Such contrasting trajectories raise questions about the evolution of cnidocytes and cnidocyte types in different cnidarian taxa, which is beyond the scope of the current study.

Neurons

Two neural cell types have been described in *Hydractinia echinata*, a sister species to *H. symbiolongicarpus*: sensory neurons and ganglionic neurons. This classification is based primarily on morphological characteristics observed using electron microscopy [31]. The two neural cell types can also be distinguished by their orientation relative to the mesoglea: ganglionic cells lie parallel to the mesoglea, whereas sensory cells are oriented perpendicular to it [22]. Together, these two neural types form the ectodermal nerve net of *H. echinata* [31]. In our single-cell atlas, two neural clusters (C7 and C14) were identified (Figs. 1c and 3a), expressing classic neural markers such as *Elav* (*HyS0085.53*, Fig. 1d) [32, 33] and *Neurocalcin* (*HyS0034.90*, Supplementary Fig. S2b-c) [34]. The neuropeptide precursor genes for *RFamide* (*HyS0013.338*) and *GLWamide* (HyS0009.155) were expressed exclusively in C7 (Supplementary Fig. S2b-c). Both markers were also expressed in a single neural cluster in Salamanca-Díaz et al. [19]. The *achaete-scute homolog* (*Ash*, *HyS0005.437*) was expressed in C14 and in developing cnidocytes (C4), similar to its expression in *Hydra magnipapillata*, where it is a known marker of sensory neurons and differentiating cnidocytes [35]. A recent *Hydractinia* single-cell atlas by Salamanca-Díaz et al. identified five neural subclusters – specifically, clusters 16, 26, 27, 29 and 33 [19]. We

compared the markers for each cluster and their expression in our atlas, and concluded that clusters C16, C27, and C29 correspond to C7 in our atlas, and clusters C26 and C33 correspond to C14 in our atlas (see final column in Supplementary Table S2).

To determine the spatial location of cells constituting the two clusters of *Hydractinia* neurons in our atlas ("Neurons A" and "Neurons B", Fig. 1c), we performed double HCR-FISH using the gene encoding for *RFamide* (*HyS0013.338*) as a marker of C7 cells (Fig. 3b) and *HyS0049.55*, a putative neuropeptide (see below) as a marker of C14 cells (Fig. 3c). Consistent with previously published results [28, 36, 37], *RFamide*$^{+}$ cells were predominantly located in the hypostome, and were present in the body column and tentacles, albeit less densely (Fig. 3d-f). In contrast, *HyS0049.55*$^{+}$ cells were predominantly located in the tentacles, revealing a previously undescribed population of neurons in the *Hydractinia* feeding polyp (Fig. 3d'-f'). We confirmed these results by using a second marker specific to C14 (*HyS0062.54*) and showed it is also expressed in cells concentrated in the tentacles (Supplementary Fig. S4a-a'"). A double HCR-FISH experiment using *RFamide* and *HyS0049.55* as probes did not show any overlap in expression (Fig. 3d"-f", d'"-f'"), similar to Fig. 3 of [28]. In that figure, a higher magnification zoom in of the tentacles is shown and DIC illumination is added to show additional detail including the proximity of cnidocytes to these neural cell types. Based on our double HCR-FISH experiments, we were unable to determine whether Neurons A and Neurons B correspond to ganglionic and sensory types based on cell orientation or other spatial or morphological information. It is possible that one or both of these two neuron types represent a mixture of ganglionic and sensory neurons, as previous studies in *Hydractinia* have indicated that both types are present in the hypostome [37, 38]. For further in-depth discussions of *Hydractinia* neurons and other cnidarian sensory cells and sensory systems, the readers are referred to our recent review paper [28]. To further investigate the morphology of the neurons expressing each of our marker genes, we performed HCR-FISH on dissociated cells (Fig. 3g-l'). We detected a range of morphologies, including tripolar neurons (Fig. 3g-g', j-j'), unipolar neurons (Fig. 3h-h', k-k'), and bipolar neurons (Fig. 3i-i', l-l') However, there was no clear distinction in the morphology of neurons from C7 and C14. Further study will be required to resolve which morphological types are present in each neuron cluster.

The nervous system of cnidarians is thought to be primarily governed by peptidergic signaling, with neuropeptides playing a role in many aspects of its biology, including metamorphosis, taxon-specific behaviors, reproduction, and feeding [39–45]. As there were no obvious morphological differences between the cells expressing our C7 and C14 markers (Fig. 3g-l'), we sought to identify the complement of neuropeptides expressed in each cluster, with the goal of identifying potential functional differences between the two neural clusters. A similar approach was taken by Chari et al. in a study of the hydrozoan jellyfish *Clytia* [14]. Using sequence-based analyses of all *H. symbiolongicarpus* gene models [18], and then filtering those predictions to exclude those that were not expressed in one or both neuron clusters of our single-cell atlas, we identified 12 putative neuropeptides, including two that were previously known (*RFamide*, *HyS0013.338* and *GLWamide*, *HyS0009.155*) and ten that were previously unidentified (Supplementary Fig. S4c-d, Supplementary Table S3). The coding sequence of one of these newly identified neuropeptides (*HyS0049.55*) was used as a C14-specific marker in experiments described above. Some of these novel neuropeptides appear to be related to those previously isolated from cnidarians. For example, *HyS0052.141* shows similarity to the PRXamide family of neuropeptides that, along with RFamides and GLWamides were likely present in the cnidarian stem lineage [46], and more specifically seems to belong to the maturation-inducing hormones (MIHs; RPRAamide peptides) [43]. MIHs have been shown to be synthesized directly by cells in the gonad in two hydrozoan jellyfish and to act directly in oocyte maturation [41]. Another neuropeptide appears to be a newly identified second member of the GLWamide class (*HyS0078.10*, Supplementary. Fig. S2, Supplementary Table S3, see [43]). Others are convincing neuropeptide precursors, but do not show clear similarity to previously described neuropeptides from cnidarians. For example, *HyS0018.64* contains 23 copies of a predicted LRLamide peptide which has been annotated as "involucrin-like" [47] but which we do not believe has been identified in any other cnidarian thus far (Supplementary Table S3). Each of the neuropeptide precursors we identified were present in one or both of the neural clusters in the single-cell atlas. This phenomenon, in which distinct combinations of neuropeptides are produced by different populations of neurons, has been observed previously in studies of the nervous system in both *Hydra* and *Clytia*, and is thought to be related to functional differences such as those related to specific behaviors [14, 45, 48, 49]. Future in-depth analyses of neural location, neurochemistry (including the presence of classical chemical neurotransmitters), and spatial and functional analyses of neurons in different polyp and tissue types within the *Hydractinia* colony will be required to fully elucidate the diversity of neuron types and neural functions in this animal.

To further investigate the neural clusters in our single-cell atlas, we subjected Clusters 7 and 14 to a subclustering analysis. After extracting C7 and C14 from the integrated dataset (Supplementary Fig. 5a), we

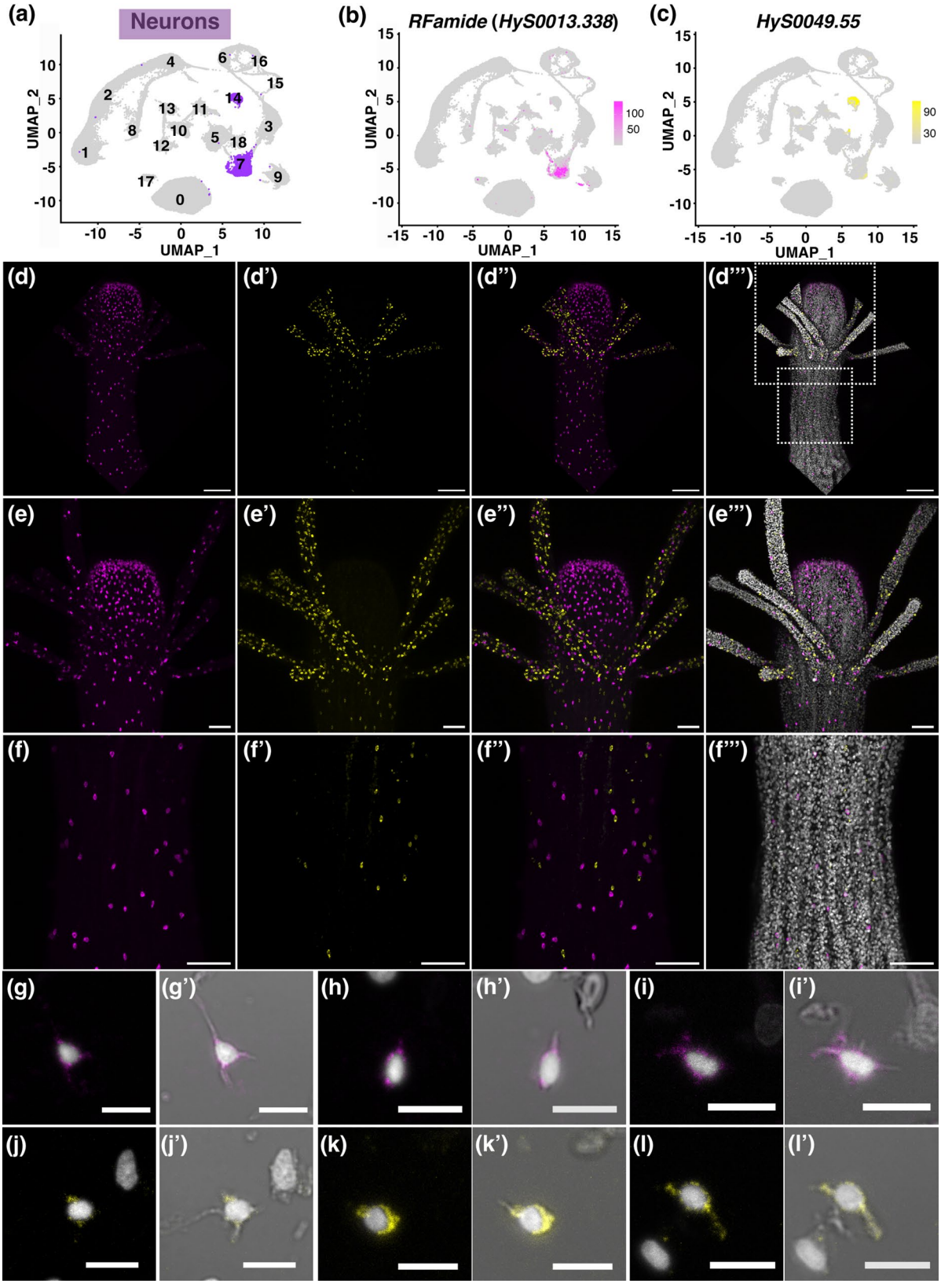

Fig. 3 (See legend on next page.)

(See figure on previous page.)

Fig. 3 Expression analysis of markers expressed in differentiated neuron cell clusters. **a** Two-dimensional UMAP of the *Hydractinia* single-cell atlas, with cluster numbers indicated and neuron clusters highlighted in purple. **b** UMAP showing expression of *RFamide* (*HyS0013.338*), which specifically marks a subset of cells in cluster 7 (magenta; this color also marks *HyS0013.338*$^+$ cells throughout the figure). **c** UMAP showing expression of *HyS0049.55*, which specifically marks the majority of cells in cluster 14 (yellow; this color also marks *HyS0049.55*$^+$ cells throughout the figure). **d**-(f‴) Confocal images of HCR-FISH of the genes shown in (**b**) and (**c**) in adult feeding polyps. The white dotted boxes shown in (d‴) indicate regions selected for higher magnification images in (**e**)-(e‴) and (**f**)-(f‴). Nuclei are shown in grey. (**g**)-(l') Cell dissociations followed by HCR-FISH show a range of neural morphologies. Scale bars: 100 µm in (**d**)-(d‴), 50 µm in (**e**)-(f‴), and 10 µm in all other panels

re-normalized and reanalyzed the data, resulting in 10 neural subpopulations visualized by UMAP (Supplementary Fig. S5b). Eight of the 10 subclusters originated from the C7 cluster, while two originated from the C14 cluster (Supplementary Fig. S5c); a list of differentially expressed genes defining the clusters can be found in Supplementary Table S4. We then plotted the expression levels of the neuropeptides previously identified in each of these neural subclusters (Supplementary Fig. S5d). In some instances, the expression of a particular neuropeptide was limited to a single cluster (e.g. *HyS0009.155/GLWamide*, C9; *HyS0055.9*, C1), while the expression of others was distributed across multiple clusters (e.g. *HyS0013.338/RFamide*, C0/C1; *HyS0051.139*, C0/C1). The number of subclusters we obtained is comparable to recent results from other hydrozoan cnidarians. For example, *Clytia* neurons have 14 subpopulations [14], and *Hydra* neurons have 11 neural subtypes [50]. In *Hydra*, these neural subtypes are also related to their position either within the ectoderm or endoderm of the polyp; eight subclusters comprise neurons present in the ectodermal nerve net, while three subclusters comprise neurons present in the endodermal nerve net. *Hydractinia* contains only ectodermal neurons, so it will be particularly interesting to resolve whether the 10 subpopulations we recovered comprise spatially distinct subpopulations within the polyp or perhaps are functionally distinct subpopulations.

Gland cells

The characterization and distribution of the different types of gland cells in *Hydractinia* polyps have not been well-studied. Studies in *Hydra* have identified two broad types of gland cells: mucous gland cells (spumous and granular) that secrete mucus, and zymogen gland cells that secrete proteolytic enzymes into the gastric cavity to enable digestion of food particles [51, 52]. Based on selected genes known to be expressed in gland cells in *Hydra* and *Hydractinia* [13, 18, 29, 53, 54], we annotated four clusters in the single-cell atlas as corresponding to the two types of gland cells: mucous gland cells (clusters C10 and C11) and zymogen gland cells (clusters C12 and C13) (Fig. 1c, Supplementary Table S2).

To determine the relative spatial locations and cellular morphology of the cells in the putative mucous and zymogen gland cell clusters and confirm their annotation, we selected a marker exclusive to the putative mucous gland cells clusters (C10 and C11), *mucin-5AC* (*HyS0004.446*, Fig. 4b, Supplementary Fig. S2c), and performed double HCR-FISH together with a previously validated gene marker for zymogen gland cells (C12 and C13), *Chitinase 1* (*Chit1*, *HyS0041.99*, Fig. 4c, Supplementary Fig. S2c) [18].

Expression analyses showed that many tightly packed *mucin-5AC*$^+$ cells were present in the gastrodermis of the hypostome, while *Chit1*$^+$ cells were distributed as expected throughout the gastrodermis of feeding polyp bodies, aboral to the hypostome (Fig. 4d-f"; [18]). The two populations – *mucin-5AC*$^+$ and *Chit1*$^+$ cells – were mostly spatially separate, except for a region at the base of the tentacles where they were adjacent, and we observed some intermixing of cell types (Fig. 4e). While there are differences among hydrozoan species regarding the distribution of mucous and zymogen gland cells in the polyp body, the most well-studied *Hydra* species contains only mucous gland cells in the gastrodermis of the hypostome and only zymogen gland cells in the gastrodermis of the polyp body [51, 52, 55], consistent with our observations in *Hydractinia* feeding polyps. This spatial separation of gland cell types was also previously reported for *Hydractinia echinata* via transmission electron microscopy [22].

The *mucin-5AC*$^+$ cells appear to exhibit two different morphologies, but their tight packing in the hypostome makes clear descriptions challenging. In general, we observed round cells with what appears to be large intracellular vacuoles (Fig. 4e", black arrowheads) and long, thin cells (Fig. 4e", white arrowheads). In *Hydra*, spumous mucous gland cells and granular mucous gland cells are morphologically and functionally distinct [13, 29, 55], so it is possible that the two morphological variants seen in *Hydractinia* correspond to these subtypes. *Chit1*$^+$ zymogen gland cells were not as tightly packed together in the gastrovascular cavity and had distinct cell boundaries, allowing us to more confidently identify the two distinct morphologies we observed. Cells were either small and round/oval (approximately 10 µm in diameter) with large nuclei (Fig. 4f", black arrowheads), or large (approximately 15–20 µm in length) with intracellular vacuoles or granules (Fig. 4f", white arrowheads). The appearance of the larger *Chit1*$^+$ cells is consistent with the known morphology of mature zymogen gland cells. The smaller *Chit1*$^+$ cells resemble a cell type observed in the gastrodermis of the hydrozoans *Halocordyle disticha* and *Hydra viridissima*, where they have been termed

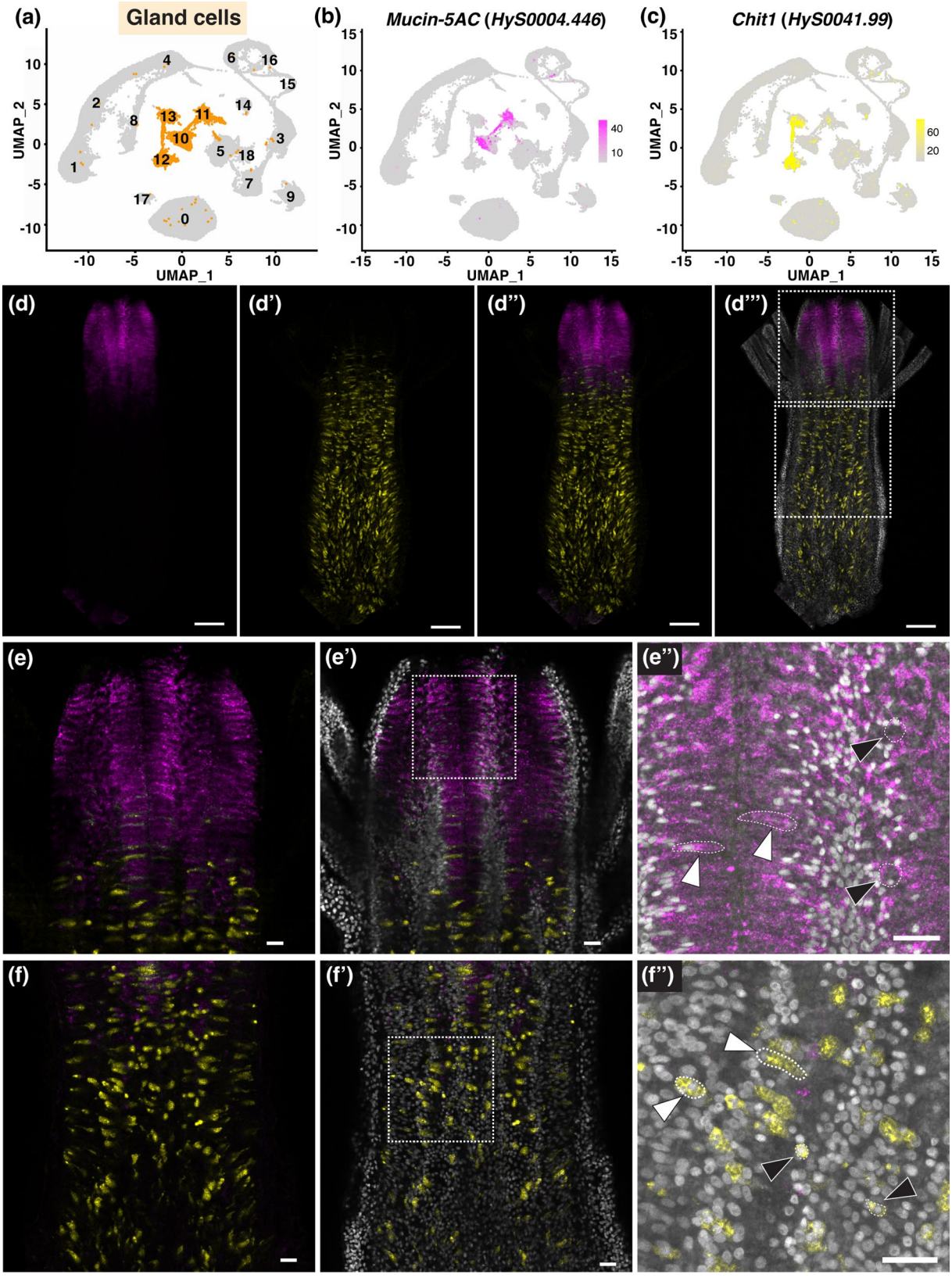

Fig. 4 (See legend on next page.)

(See figure on previous page.)

Fig. 4 Expression analysis of markers expressed in differentiated gland cell clusters. **a** Two-dimensional UMAP of the *Hydractinia* single-cell atlas with cluster numbers indicated and gland cell clusters highlighted in orange. **b** UMAP showing expression of the mucous gland cell marker *mucin-5AC* (*HyS0004.446*) (magenta; this color also marks *HyS0004.446*$^+$ cells throughout this figure). **c** UMAP showing expression of the zymogen gland cell marker *Chit1* (*HyS0041.99*) (yellow; this color also marks HyS0041.99$^+$ cells throughout this figure). **d**-(f''). Confocal slices of an HCR-FISH in the gastrodermis of adult feeding polyps, showing expression of the genes shown in (**b**)-(**c**). Nuclei are shown in grey. **d**-(d''') shows a whole adult feeding polyp, while (**e**)-(e'') shows a higher magnification image of the hypostome and (**f**)-(f'') shows a higher-magnification image of the polyp body. Dotted white boxes in (d''') indicate the regions of higher magnification images shown in (**e**-e'') (upper white dotted box) and (**f**-f'') (lower white dotted box). Dotted white boxes in (e') and (f') indicate the regions shown at higher magnification in (e'') and (f''), respectively. Images in (e'') and (f'') are confocal slices overlaid with transmitted light images. White arrowheads in (e'') indicate examples of long, elongated *mucin-5AC*$^+$ cells, while black arrowheads in (e'') indicate smaller, rounder *mucin-5AC*$^+$ cells. White arrowheads in (f'') indicate examples of large *Chit1*$^+$ cells with intracellular granules, while black arrowheads indicate examples of small, rounded *Chit1*$^+$ cells. Scale bars: 100 µm in (**d**)-(d''') and 20 µm in all other panels

"young zymogen cells", "undifferentiated gastrodermal cells", or "basal reserve cells" [22, 51, 52, 56]. These cells were described as oval in shape, 10–12 µm in diameter, and were hypothesized to be either immature zymogen gland cells, a zymogen gland cell following secretion of their granules, or a dedifferentiated zymogen gland cell [51, 52]. In the gastrodermis of the stolons and budding feeding polyps in young *Hydractinia* colonies, we have observed that almost all *Chit1*$^+$ cells are of this smaller type (unpublished data), suggesting that these cells might indeed be precursors of mature zymogen gland cells.

It is possible that the two mucous gland cell clusters correspond to spumous and granular mucous gland cells as described in *Hydra* [55]. For example, *mucin2-like* (*HyS0015.116*) is restricted to cluster 10 (Supplementary Fig S2c) and it's probable ortholog in *Hydra* is specifically expressed in spumous mucous gland cells (G010426) [29]. *Rhamnospondin* (*HyS0004.396*) is specifically expressed in cluster 11 (Supplementary Fig. S2c) and likely plays a role in immune recognition [54], suggesting a functional difference between cells in C10 and C11. Conducting multi-color spatial expression analyses with markers exclusive to each of the four gland cell clusters will allow us to further investigate these clusters and their contributions to both zymogen and mucous gland cell populations in *Hydractinia* feeding polyps. For example, we have identified several markers with high transcript levels that would make ideal candidates for HCR-FISH analysis; *HyS0021.97* along with *mucin2* (*HyS0015.116*) for cluster 10, *HyS0118.19* along with *Rhamnospondin* (*HyS0004.396*) for cluster 11, *HyS0011.72* and *HyS0045.34* for cluster 12 and *HyS0042.129* and *HyS0001.383* for cluster 13.

Epithelial cells

Cnidarian epithelial cells are known to be multifunctional [57–59] and many names have been used in the past to refer to subtypes, such as epitheliomuscular cells (EMCs) [31, 58, 60] and digestive muscular cells [22]. We defined the two major epithelial cell clusters based solely on tissue layer location: endodermal (C0 and C17) and ectodermal (C5), while acknowledging their multifunctionality (Figs. 1c and 5a). A marker for C0 and C17, *Astacin 3* (*HyS0078.51*, Fig. 5b, Supplementary Fig. S2c) [61], was expressed in the endoderm along the entire polyp body, including in the endodermal cells of the tentacles (Fig. 5d-f'''). A specific marker for C5, *Fat 1* (*HyS0048.57*, Fig. 5c), was expressed in cells in the ectoderm along the entire body of the feeding polyp, as well as in the tentacles (Fig. 5d-f'''). C17 may constitute a subpopulation of the endodermal epithelial cells, and future studies could use C17-specific genes in spatial experiments (Supplementary Table S5). Ectodermal epithelial cells have been shown to have more prominent myofibrils than the endodermal epithelial cells in *Hydractinia* and were hypothesized to be the main drivers of muscular contraction [62]. In support of this hypothesis, we found more cells that expressed muscle-related genes in C5 compared to C0 and C17, such as the genes encoding for the myosin heavy chain structural protein (*HyS0006.325*) and the myosin light chain kinase (*HyS0028.60*) (Supplementary Fig. S6a). In contrast, the most significant Gene Ontology for C0 was "GO:0006508, proteolysis" (Supplementary Fig. S6b), consistent with previous descriptions of a digestive function for gastrodermal epithelial cells [22]. Notably, many genes in the major endodermal epithelial cluster (C0) showed a gradient expression pattern within the cluster (e.g. *HyS0008.375*, *HyS0021.141*, *HyS0034.215*, *HyS0087.37* and *HyS0244.2*) (Supplementary Fig. S6c). Similarly, in *Hydra*, some epithelial cell marker genes displayed graded patterns depending upon their position along the oral-aboral axis [13]. Further *in situ* hybridization experiments with these and other genes will be needed to confirm the hypothesis that the graded expression level of genes in this cluster is related to spatial expression patterns along the oral-aboral axis in feeding polyps.

We also identified a cluster adjacent to C5 in the atlas (C18) that appeared to be a subtype of ectodermal cells (Fig. 1c). Among the differentially expressed genes in this small cluster was *frizzled 3* (*HyS0103.16*), a gene previously reported to be expressed only in stolons (Supplementary Table S5, Supplementary Fig. S2b-c) [63]. In addition, *chitin synthase* (*HyS0024.60*) was also highly expressed in C18. Chitin is a major component of the periderm that covers *Hydractinia* stolon tissue, but not

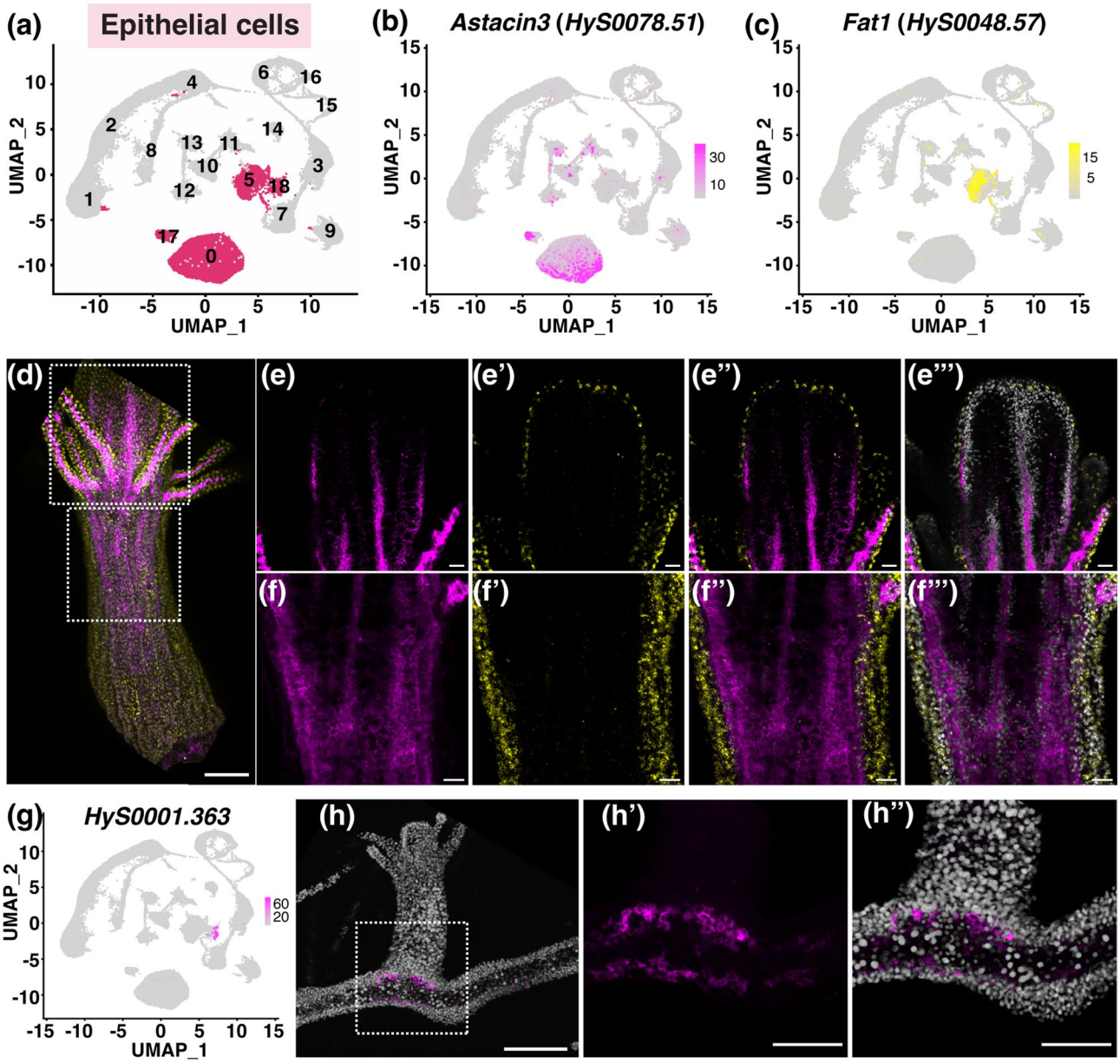

Fig. 5 Expression analysis of markers expressed in epithelial cell clusters. **a** Two-dimensional UMAP of the Hydractinia single-cell atlas with cluster numbers indicated and epithelial cell clusters highlighted in maroon. **b** UMAP expression of Astacin3 (HyS0078.51) highlighted in magenta that marks endodermal epithelial cells. **c** UMAP expression of Fat1 (HyS0048.57) highlighted in yellow that marks ectodermal epithelial cells. **d**-(f''') Confocal sections of in situ hybridization patterns in an adult feeding polyp of the genes shown in (**b**)-(**c**). Astacin3 (HyS0078.51) expression is shown in magenta and Fat1 (HyS0048.57) expression is shown in yellow. Nuclei are shown in grey. **d** Maximum projection of confocal slices of an adult feeding polyp. White dotted boxes indicate the location of the higher magnification images shown in (**e**)-(e''') (upper box) and (**f**)-(f''') (lower box). **g** UMAP expression of HyS0001.363 that marks stolon-specific ectodermal epithelial cells highlighted in magenta. **h**-(h'') Expression of HyS0001.363 in the stolon at the base of a young feeding polyp shown in magenta. Nuclei are shown in grey. The white dotted box in (**h**) represents the region of the higher magnification image selected for (h')-(h''). Scale bars: 100 µM in (**d**), 20 µM in (**e**)-(f'''), 100 µm in (**h**), and 50 µm in (h')-(h'')

polyps [3, 64]. This led us to hypothesize that the cells in cluster C18 are stolon-specific epithelial cells. To confirm this, we conducted HCR-FISH with a gene of unknown function that is highly specific to C18, *HyS0001.363* (Fig. 5g) and found it was specifically expressed at the base of young polyps where they intersected with the stolon (Fig. 5h-h''). Another recent *Hydractinia* single-cell atlas [19] also identified a stolon-specific epithelial cell cluster, and we cross-checked several stolon-specific markers from their cluster with those identified in this study, finding a high level of similarity. For example, the homolog of *HyS0001.363* (*LOC130636562*) is specifically expressed in the stolon-specific cluster in the atlas from [19], and the best match to the highly repetitive *prisilkin/*

shematrin-like genes identified in the stolon-specific cluster in that atlas is *HyS0026.224*, which is specific to C18 in our atlas. Further investigation of the origin of these stolon-specific cells during *Hydractinia* metamorphosis and development, as well as analysis of the evolutionary conservation of the genes specifically expressed in this cluster, may lead to a greater understanding of the evolution of coloniality.

Putative immune cells

The immune gene repertoire of *Hydractinia* was predicted to be large but no immune cell types have been described to date [65]. In an initial attempt to assign a putative function to cluster C9 (Figs. 1c and 6a), we performed GO enrichment analysis. The top Gene Ontology hit was to "peptidyl-tyrosine dephosphorylation" (GO:0035335) (Fig. 6b). Over half of the tyrosine phosphatases encoded in the human genome are expressed by immune cells [66], which led us to suspect immune related functions of this cluster.

Exploring the list of differentially expressed genes reveals further intriguing hints as to the potential function of the cells in this cluster. For example, one of the top differentially expressed genes is *conodipine-like* (*HyS0053.57*) (Supplementary Table S5), which contains a phospholipase A2 (PLA2) domain (InterPro entry IPR036444) and a signal peptide (as predicted by SignalP v6.0). Secreted PLA2 enzymes can release free fatty acids from phospholipids [67]. These enzymes, which are expressed by human inflammatory cells such as macrophages and T-cells, possess antibacterial and antiviral properties [68]. A second intriguing gene present in this cluster is an *interferon regulatory factor 1 (Irf)-like* gene (*HyS0045.75*) (Supplementary Table S5, Supplementary Fig. S2c). Irf proteins are involved in the immune response in a wide variety of animals [69] and were recently identified as being expressed in immune cells in the anthozoans *Nematostella*, *Stylophora*, and *Acropora* [15, 31, 70, 71]. Other differentially expressed genes of this cluster also included an *Alr1-like* gene (*HyS0029.183*) (Supplementary Fig. S2c) and *Alr2* (*HyS0001.708*) (Supplementary Table S5), but not *Alr1* (*HyS0031.168*). *Alr1/2* genes encode transmembrane proteins that are vital for self/non-self recognition between *Hydractinia* colonies [69–71], while the related *Alr1-like and Alr2-like* genes, which are also present in the allorecognition complex of *Hydractinia*, have been hypothesized to play a role in the anti-pathogenic immune response, separate from their role in self/non-self recognition [72].

We conducted HCR-FISH on feeding polyps to determine the location and morphology of cells in cluster C9 using three specific markers; *HyS0016.300*, an unannotated gene (Fig. 6c), and the previously discussed genes *Irf-like* (*HyS0045.75*), and *conodipine-like* (*HyS0053.57*) (Supplementary Fig. S7a-b). Each of these markers were predominantly expressed in cells of the ectoderm, distributed widely over the polyp body, including within some cells in the tentacles and hypostome (Fig. 6d-f, Supplementary Figs. S7a'-a''' and b'-b'''). In approximately half of the polyps, each marker also showed expression in one or more connected group of cells (upper box in Fig. 6d, higher magnification image in Fig. 6e-e'). The biological significance of these connected groups is unclear.

The morphology of cells expressing *Hy0016.300* was varied. We obtained high-magnification images of individual cells from whole-mount HCR-FISH samples (Fig. 6g-i') and also performed HCR-FISH on dissociated cells (Fig. 6j-l'). Some cells were elongated with a central nucleus (Fig. 6g-g', j-j'), others were round (Fig. 6h-h', k-k'), while others were irregularly shaped (Fig. 6i-i', l-l'). Cells that expressed either *Irf-like* or *conodipine-like* showed less morphological diversity and were generally round (Supplementary Fig. S7a'-a''' and b'-b'''). It is unclear if this morphological diversity indicates cells within cluster C9 consist of more than one cell type or whether cells within this cluster change their shape for biological reasons (e.g., due to cell migration or phagocytosis).

A discrete cluster of cells with transcriptomic characteristics similar to cluster C9 in our atlas was also identified in Salamanca-Díaz et al. [19]. In that atlas, these cells were labeled as "conodipine+" or, alternatively, as "venomous epithelial cells." Using immunofluorescence targeting Alr1 (LOC130635932), the authors report that these cells are widespread in the ectodermal epithelial layer of feeding polyps at the aboral end of the polyp and in the stolon. However, *Alr1* (LOC130635932) is not specifically expressed in the "conodipine+" or "venomous epithelial cell" cluster in their atlas; instead, it is rather widespread. Similarly, *Alr1* (*HyS0031.168*) is also not specifically expressed in cluster C9 in our atlas, but instead is broadly expressed across the entire UMAP. The *Alr1-like* gene (LOC130635943) shown in Fig. 5B of that study would not be recognized by the specific Alr1 antibody used to generate the images in their Fig. 5C. Therefore, the immunofluorescence pattern of the Alr1 antibody shown in [19] and the HCR-FISH patterns for the genes we used to highlight our C9 cluster (*HyS0016.300*, *conodipine-like*, *and Irf-like*) cannot be directly compared or expected to give similar spatial patterns.

Salamanca-Díaz et al. identified cluster 36 as another cluster that expressed *conodipine-like* genes (e.g. *LOC130636858* and *LOC130642091*). We compared the expression of some markers differentially expressed and specific to cluster 36 of Salamanca-Díaz et al. to the expression of their homologs in our atlas, (e.g. *LOC130624087/HyS0023.319* and *LOC130653886/HyS0010.146*) and find that it is likely that cluster 36

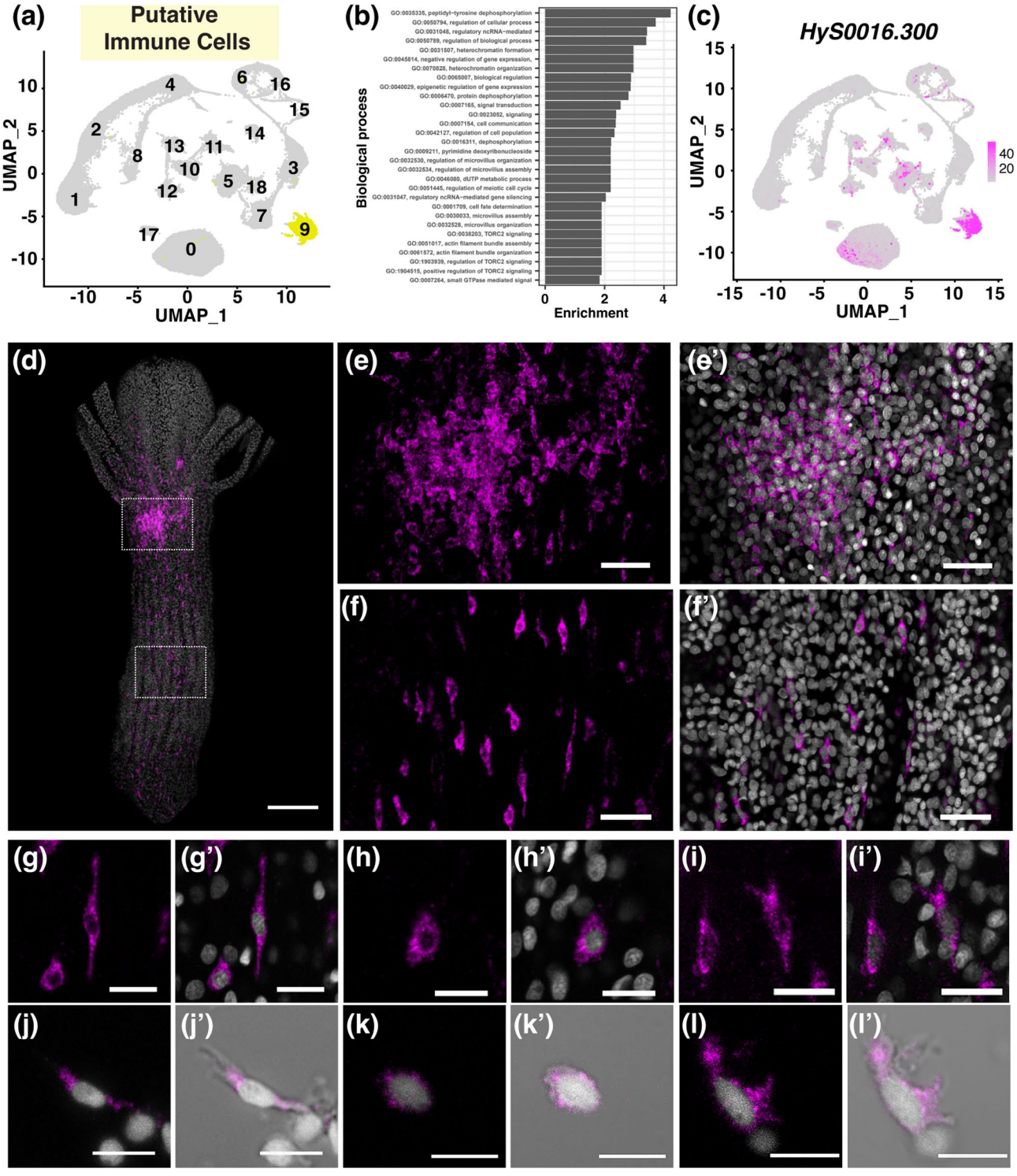

Fig. 6 Expression analysis of markers expressed in cluster 9, which are putative immune cells. **a** Two-dimensional UMAP of the *Hydractinia* single-cell atlas with cluster numbers indicated and cluster 9 highlighted in yellow. **b** Top Gene Ontologies associated with differentially expressed marker genes for cluster 9. **c** UMAP expression of *HyS0016.300* highlighted in magenta. **d** Maximum projection of confocal sections of a whole adult feeding polyp. Dotted white boxes show regions of higher magnification images shown in (**e**)-(e') (upper box) and (**f**)-(f') (lower box). *HyS0016.300*$^{+}$ cells are shown in magenta, and nuclei are shown in grey. **g**-(i') High-magnification images of confocal sections of *HyS0016.300*$^{+}$ cells from an adult feeding polyp illustrating different cell morphologies. **j**-(l') Cell dissociation followed by HCR-FISH also reveals a range of *HyS0016.300*$^{+}$ cell morphologies. Scale bars: 100 µm in (**d**), 20 µm in (**e**)-(f'), and 10 µm in all other panels

from that study is equivalent to a subset of cells within our neural subcluster C7. Another cluster in Salamanca-Díaz et al. (C13) is designated as "*Conodipine+/Avidin+*" and likely corresponds to the endodermal epithelial cell clusters (C0/C17) in our atlas, based on the expression of marker genes such as *LOC130646270*/*HyS0053.113 (Avidin-like*) and *LOC130629039/HyS0035.54*.

Taken together, bioinformatic and marker gene expression analyses have led us to hypothesize that the cells comprising C9 represent a distinct type of ectodermal cell specifically involved in host defense and immunity in *Hydractinia*. These cells might be involved in the identification of pathogens and/or the downstream responses that potentially involve phagocytosis and intracellular digestion. Epithelial cells in *Hydra* [73] and anthozoan amoebocytes have been shown to be phagocytic and, in some cases, migratory [74–77]. Ultimately, determining the precise function of the cells that constitute cluster C9 will require further experimentation that is beyond the scope of this study. For example, future experiments could investigate the response of these cells when *Hydractinia* is exposed to pathogenic organisms or other non-self challenges. Additionally, phagocytosis assays could be performed.

I-cells and progenitors

I-cells are adult stem cells in *Hydractinia*. They are found throughout the colony, including in feeding polyps, sexual polyps, and the stolon. In feeding polyps, they are located primarily in the epidermal layer and are most dense in a band-like region in the aboral half of the polyp body. They are characterized by their size (7–10 μm), large nuclear-to-cytoplasmic ratio, and high ribosomal content [8]. The C3 cluster was annotated as i-cells and progenitors due to the expression of known i-cell markers such as *Piwi1* (*HyS0050.7*, Supplementary Fig. S2c), *Myc (HyS0005.84*), and *Nanos1* (*HyS0036.26*) [8]. C3 was connected to one of the neural clusters (C7) and three cnidoblast clusters (C6, C15, C16), cell types that are known to differentiate from i-cell precursors (Fig. 1c) [78].

To further investigate the i-cell population, we performed a subclustering analysis to determine whether the C3 cluster might contain transcriptionally distinct subpopulations. After subsetting C3 from the larger dataset (Fig. 7a), we re-normalized the data and generated t-SNE plots for visualization, resulting in five subclusters (Fig. 7b). We then used CytoTRACE to examine the differentiation state of cells that formed the different subclusters from early (blue/green) to late (orange/red) (Fig. 7c). Using a similar approach to the one we applied to the full UMAP, we annotated these subclusters using the top differentially expressed genes of each cluster (Supplementary Table S6), combined with literature searches to identify genes that had previously identified functions in *Hydractinia*, other cnidarians, and other animals (Fig. 7b).

The canonical i-cell marker, *Piwi1*, was predominantly expressed in the largest subcluster (cluster 0; Fig. 7b, d). Genes that showed differential expression in this cluster also included those involved in ribosome biogenesis, such as *NOP56* (*HyS0073.68*), *NOP58* (*HyS0155.10*) [10], and *GNL3* (*HyS0059.86*, Supplementary Fig. S2c) [79], as well as genes encoding ribosome subunits *RPL38* (*HyS0006.38*) and *RPL23* (*HyS0023.266*) (Fig. 7d, Supplementary Table S6). Given that *Hydractinia* i-cells have been described as "rich in ribosomes" [8] – a feature shared with mammalian embryonic stem cells that are also known to display elevated ribosomal gene expression (reviewed in [80]) – as well as the high levels of *Piwi1* observed in this cluster, we labeled this subcluster as the true i-cells.

The second largest subcluster (cluster 1, Fig. 7b), expressed known marker genes for cnidoblasts, *NR2E1* (*HyS0022.107*, Fig. 7d) [13], *Txd12* (*HyS0042.111*) and *Fkbp14* (*HyS0020.22*) (this publication), as well as genes involved in the DNA replication machinery, including *PCNA* (*HyS0061.60*, Fig. 7d) [10] and *MCM7* (*HyS0009.219*). Cnidocytes are single-use cells that are required to be constantly replenished via cell division from i-cell precursors. Therefore, the presence of specific cnidoblast markers combined with genes involved in cell proliferation led us to label this cluster as cnidoblasts. Next, we annotated two subclusters as neuroblasts (clusters 2 and 4, Fig. 7b), based on expression of neurogenesis genes such as *Neurogenin* (*HyS0028.205*) and *Sox22* (*HyS0012.308*) (Fig. 7d). A final cluster remained unannotated (cluster 3 "unknown", Fig. 7b) due to having a very short list of differentially expressed genes (Supplementary Table S6). CytoTRACE analysis of the entire i-cell subcluster showed that the cells of this cluster were more differentiated compared to cells in other subclusters, indicating that it might contain progenitor cells of a yet unidentified cell type or represent a transitory state between two cell types (Fig. 7c).

We did not identify a subpopulation of cells in C3 that could serve as progenitors to epithelial or gland cells. These progenitor cells may be present in the unannotated subcluster or exist in very low numbers, making them undetectable at the current clustering resolution. In *Hydra*, it has been shown that, unlike cnidocytes, epithelial and gland cells have a slower turnover rate [81–83]. The absence of lineage connections between i-cells and these cell types in the atlas presented here, as well as in previous single-cell atlases [18, 19], suggests that the same is true for *Hydractinia*.

Genes such as *Piwi1*, *Myc*, and *Nanos1* have long been used as markers for i-cells and pluripotency in *Hydractinia* [8, 9]. A recent article detailing the migration of a

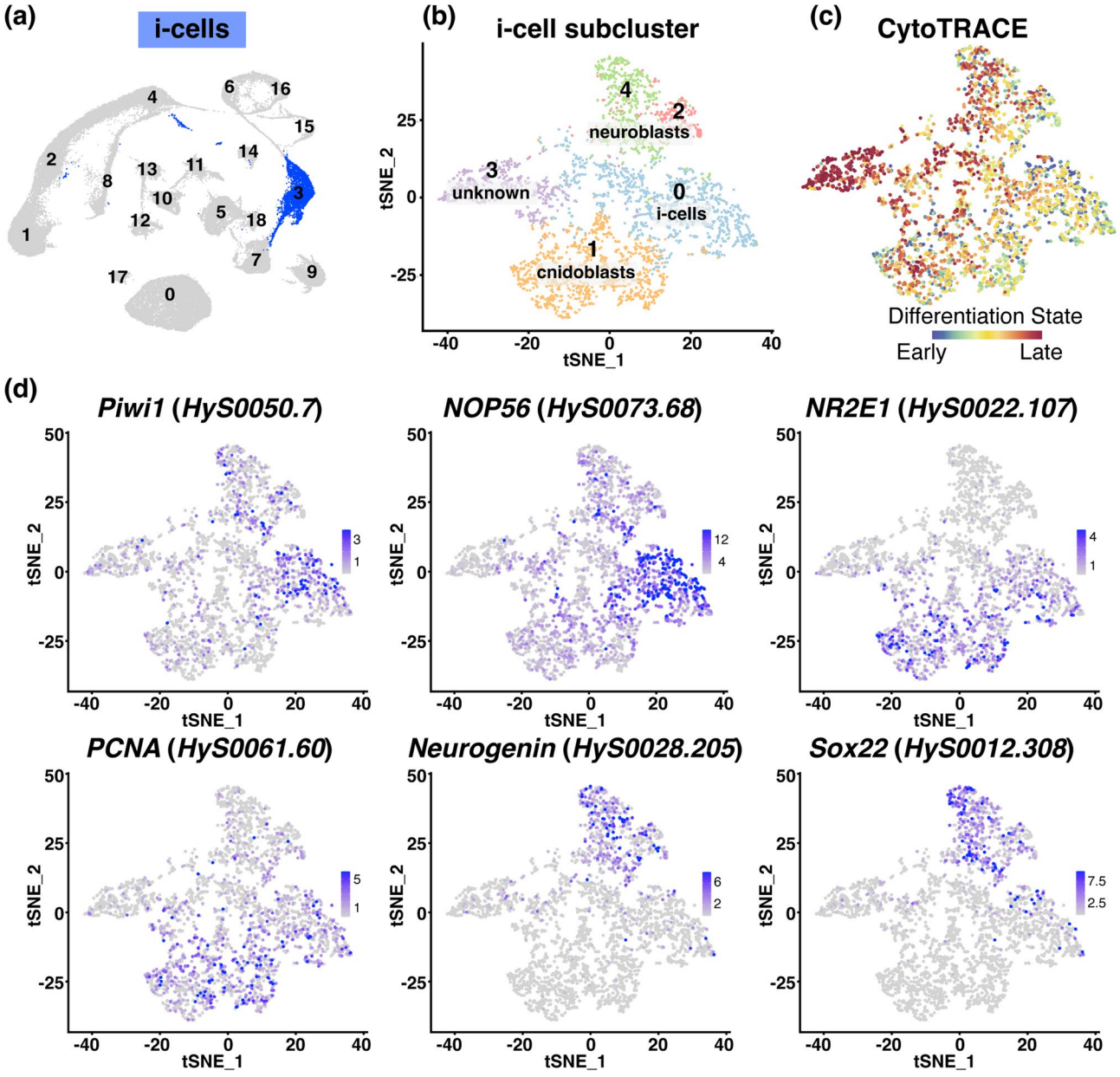

Fig. 7 I-cell and progenitors subclustering analysis. **a** Two-dimensional UMAP of the *Hydractinia* single-cell atlas with cluster numbers indicated and cluster 3 (i-cells/progenitor cells) highlighted in blue. **b** The i-cell cluster was selected and reclustered to generate the i-cell subcluster atlas resulting in five clusters. We designated three putative cell states to these clusters with the identity of one cluster remaining unknown. **c** CytoTRACE analysis was performed on the i-cell subcluster object, revealing the differentiation state from early (blue/green) to late (orange/red). **d** UMAP expression of specific genes that were used to annotate the clusters in (**b**)

single *Piwi1-GFP*$^{+}$ cell and subsequent proliferation and differentiation into all cell types provided direct evidence for their pluripotency [78]. In the i-cell subclustering analysis detailed here, *Piwi1* expression was predominantly localized to one subcluster; however, it was not exclusive to that subcluster – for example, neuroblast subcluster cells also express *Piwi1* (Fig. 7d). This parallels findings in other highly regenerative organisms, such as planarians, where lineage-primed progenitors (including neural-specified neoblasts) retained pluripotency [84, 85]. These observations suggest that, while *Piwi1* is a useful marker, it alone cannot fully define adult stem cell identity. Instead, our results support a model where adult stem cells likely comprise a heterogeneous population that includes both undifferentiated and lineage-primed progenitors, with dynamic gene expression that adapts to cellular contexts [86].

Conclusions

Here, we present an updated and spatially validated somatic single-cell atlas for *Hydractinia* feeding polyps and stolons. By integrating a previously published live-cell dataset with newly generated fixed-cell datasets, we comprehensively recapitulate all known cell lineages – except the germline – while expanding the current understanding of *Hydractinia*'s cellular landscape. Key discoveries include the identification of a novel neural subtype (Neurons B) primarily found in tentacles, two spatially distinct gland cell populations resembling those found in *Hydra*, and a putative immune cell type. We provide the first complete cnidogenesis trajectory for *Hydractinia*, validating the expression of key markers along this pathway that splits into two distinct terminal endpoints representing desmonemes and euryteles. This trajectory enables comparative analysis with existing trajectories from *Hydra*, *Nematostella*, and *Clytia*, offering new insights into the evolution of this specialized cnidarian cell type. We also re-clustered the somatic i-cell population and successfully identified distinct subclusters, assigning putative cell states to each. This analysis uncovered a population of *bona fide* i-cells, along with early progenitor populations for specific cell types that will be useful in exploring the transcriptional dynamics governing stem cells and early progenitors. Notably, the absence of shared neuroglandular progenitors in our atlas aligns with findings in *Clytia* but contrasts with those from *Hydra* and *Nematostella*; further studies incorporating young or regenerating polyps could clarify the relationship between neurons and gland cells in *Hydractinia*. Future work could also focus on characterizing the putative immune cell type through pathogen challenges and phagocytosis assays. This updated atlas provides a wealth of new data, promising candidate genes for creating transgenic reporter lines, and a foundation for deeper characterization of specific cell types and cell states through targeted functional investigations.

Materials and methods

Animal husbandry

Adult *Hydractinia symbiolongicarpus* colonies (291 – 10, male) were maintained at the University of Florida, Whitney Laboratory for Marine Bioscience. Colonies were grown on glass microscope slides and cultured in 38 L tanks filled with artificial seawater (Coral Pro Salt, Red Sea) at 30 ppt and kept at 18–20 °C under a 10 h/14 h light/dark regime. Animals were fed five times a week with 3-day-old brine SEP-Art *Artemia* nauplii (INVE Aquaculture), which were enriched two times with S.presso (SELCO) the day before colony feeding.

Single-cell dissociation

Protocol was adapted from a previous *Hydractinia* single-cell study [18]. Twenty feeding polyps (gastrozooids) and their surrounding stolonal tissue were removed from the colony and washed three times in calcium- and magnesium-free seawater (CMFSW: 450 mM NaCl, 9 mM KCl, 30 mM Na_2SO_4, 2.5 mM $NaHCO_3$, 10 mM Tris-HCl, 2.5 mM EGTA, 25 mM HEPES). The polyps and stolon were then placed in 300 µL 1% pronase (Santa Cruz Biotechnology, catalog # sc-264144) in CMFSW for 1.5 h on a rocker at room temperature. Every 15 min the tube was gently mixed by inverting. Once the tissue was fully dissociated, the cell suspension was filtered using 70 µM Flowmi tip filter (Bel-Art, catalog # H13680-0070) into a 2 ml DNA LoBind tube (Eppendorf, catalog # 022431048). The sample was centrifuged at 300 g for 5 min at 4 °C. Supernatant was gently removed while leaving about 50 µL at the bottom of the tube, then 500 µL CMFSW was added to resuspend the cell pellet. The sample was centrifuged again at the same settings above, supernatant removed and resuspended in 200 µL CMFSW. Cells concentrations were determined using a hemocytometer.

Cell fixation

Dissociated cells were then immediately fixed using two different fixatives: 800 µL ice-chilled 100% methanol (Sigma-Aldrich) or ACME solution (13:3:2:2 ratio of DNase/RNase-free distilled water, methanol, glacial acetic acid, and glycerol) [87]. Both fixatives were added dropwise to the cell sample. Fixed cells were then transferred to a –20 °C freezer for storage.

Single-cell RNA sequencing

Fixed single cell samples were diluted to 1,000 cells µL and shipped on dry ice to the National Institute of Health Intramural Sequencing Center (Bethesda, Maryland, USA). Cells were thawed, spun, and resuspended but cell counts were not obtained again, and the samples were loaded into the 10X Genomics platform for encapsulation with the capture target of 3,000–9,000 cells per sample (Supplementary Table S1). Sequencing libraries were prepared according to the standard 10X Genomics V3 chemistry protocol. The cDNA libraries were pooled and sequenced as 150 bp paired end reads and single indexed on an Illumina NovaSeq6000 with 63 million projected clusters per sample. Raw sequencing data were processed with the Cell Ranger v7 pipeline (10X Genomics), using default parameters and expected recovery of 3,000–9,000 cells for each respective library. The "Hsym_primary_v1.0" genome was used for mapping and can

be downloaded from National Center for Biotechnology Information (NCBI) (https://www.ncbi.nlm.nih.gov/datasets/genome/GCA_030121725.1/) or the *Hydractinia* Genome Project Portal (https://research.nhgri.nih.gov/hydractinia/).

Data processing and bioinformatic analyses

After preliminary QC in Cell Ranger, one of the ACME-fixed samples was discarded due to poor quality. In addition to the two methanol-fixed samples and seven remaining ACME-fixed samples, we also included a previously published single-cell dataset of *Hydractinia symbiolongicarpus* in our analyses [18]. To focus on somatic cell lineages, cells expressing sperm-related markers (*HyS0027.170*, *HyS0070.46*, *HyS4524.1*, *HyS0007.253*, *HyS0001.110*) were removed from the previous dataset. All count matrices were individually processed and cleaned using Seurat v5.2.1 [88, 89] in R. In short, potential cell multiplets were removed by using a library-specific cutoff for aberrantly high UMI counts and gene counts (for detailed sample processing, see code in "Data Availability"). After the initial filtering, we ran the dataset through a standard Seurat analysis pipeline using the default parameters unless otherwise specified as follows: data were normalized and variable features were selected by running *SCTransform*(vst.flavor = "v2") [90]. The top 50 principal components were calculated with the *RunPCA* function. Clustering was performed by running the *FindNeighbors* function with dims = 1:15. This was followed by running *FindClusters* with resolution = 0.5. Nonlinear dimensionality reduction was performed to represent the data in a 2D space using Uniform Manifold Approximation and Projection (UMAP) [91].

Given that all our samples are predicted to include most cell types of the animal, and no significant technical variation was expected, we chose canonical correlation analysis (CCA) to integrate different datasets [92]. We selected 3,000 genes by running *SelectIntegrationFeatures* and integrated datasets by running *IntegrateData*, normalization.method = "SCT". The integrated dataset was then processed using the standard Seurat pipeline above, with 50 principal components, dims = 1:20 in clustering and resolution = 0.3 in UMAP. Differential expression (DE) analyses were identified with the *FindAllMarkers* function, with min.pct = 0.1, min.diff.pct = 0.5, logfc.threshold = 1, using the "RNA" assay. Clusters were annotated based on the DE gene list and known cell type markers [18]. A list of genes used to annotate all the clusters can be found in Supplementary Table S2 and their expression in the single-cell atlas shown as Supplementary Fig. S2b-c.

Cnidogenesis single-cell atlas

The updated *Hydractinia* single-cell atlas was subset to create a cnidogenesis atlas using R (v4.4.0) and the Seurat v5.1.0 package [89]. I-cells and cnidocyte clusters (C1, C2, C3, C4, C6, C8, C15, and C16) were extracted from the whole Seurat single-cell object to create a cnidogenesis specific object. Integration anchors were calculated to reduce batch effects from the different single-cell libraries. Finally, dimensionality reduction and clustering analysis were performed to generate the final version of the *Hydractinia* cnidogenesis single-cell atlas. To align the orientation of the cnidogenesis differentiation trajectory in the whole atlas with the cnidogenesis atlas trajectory, the x-axis of the cnidogenesis atlas dimensionality reduction plots (e.g., *FeaturePlot*, DimPlot) were reversed using scale_x_reverse() in the ggplot2 package [93].

CytoTRACE differentiation state analysis

The R package CytoTRACE v0.3.3 was used to predict the differentiation state of cells in the *Hydractinia* cnidogenesis single-cell atlas and the i-cell subcluster atlas [94]. Differentiation scores for each cell were computed, added to the metadata of the relevant Seurat object, and then visualized using the Seurat *FeaturePlot* function. The CytoTRACE differentiation scores were inverted so that less differentiated cells had lower scores, and more differentiated cells had higher scores.

Monocle3 trajectory and pseudotime analysis

The cnidogenesis Seurat object was converted into a Monocle3 (v1.3.7) cell data object [95] and original Seurat PCA and UMAP embeddings were manually added to the metadata. The cellular trajectory was predicted using the learn_graph function and pseudotime was estimated by manually selecting the i-cell cluster as the root.

Gene ontology

Gene ontology enrichment analysis was performed and visualized using the R package topGO v.2.54.0 [96]. The corresponding GO term accessions were retrieved from a customized text file (supplement "Hsym_v1.0_GO_terms.out") for *Hydractinia*. Genes of interest were the differentially expressed genes from each cluster (Supplementary Table S5). Enrichment tests were performed using the arguments algorithm='classic', statistic='fisher'.

Neuron subcluster analysis

Clusters 7 and 14 were extracted from the Seurat integrated dataset for further subclustering. The subset was re-normalized using *SCTransform* (vst.flavor = "v2"), and dimensionality reduction was performed with PCA.

Clustering was carried out using the first 15 principal components, with a resolution of 0.1, followed by UMAP visualization. Differential expression analyses were performed using the *FindAllMarkers* function on the RNA assay, with min.pct = 0.3 and logfc.threshold = 1 (Supplementary Table S4).

Neuropeptide predictions

Putative neuropeptides were predicted based on the method in [14]. *Hydractinia* predicted proteins were downloaded from the genome project portal (https://research.nhgri.nih.gov/hydractinia/) and screened for the presence of a signal peptide using SignalP v6.0 [97]. Proteins deemed to be transmembrane proteins were removed, based on predictions from SignalP v4.0. A custom Perl script (process_signalp4_and_6_outputs.pl) was then implemented to screen the remaining proteins that possessed a signal peptide for the presence of one or more neuropeptide cleavage sites (G[KR][KRED]). When more than one site was present, the 6 residues immediately N-terminal to this cleavage site were compared with each other. Putative neuropeptides were ranked according to a normalized score, where the sum of identical amino acids at each position for each 6 AA motif were divided by the number of motifs present in a protein. Expression profiles of all putative neuropeptides in the single cell atlas were then investigated. Those that had a normalized score of 1 or more that were also expressed predominantly in one or both neural clusters (clusters 7 and/or 14) were selected. This shortlist was further refined by manually comparing the 6 amino acid motifs within each protein to each other to ensure similarity. Finally, a list of 12 putative neuron-specific neuropeptides was generated. UMAP embeddings of each of these genes are shown as Supplementary Fig. S4, and amino acid sequences shown as Supplementary Table S3.

I-cell/progenitors subcluster analysis

Cluster 3 was subjected to further subclustering analysis to investigate potential cell subpopulations. The three datasets were SCTransformed (vst.flavor = "v2") individually as mentioned above and reintegrated using CCA with 3,000 features (genes). The integrated dataset was then processed using the standard Seurat pipeline, with 25 principal components, dims = 1:25 in clustering and resolution = 0.2 in t-SNE projection. Differential expression (DE) analyses were identified with the *FindAllMarkers* function, with min.pct = 0.3, logfc.threshold = 1, using the "RNA" assay (Supplementary Table S6).

HCR fluorescent *in situ* hybridization (HCR-FISH)

For each cell cluster, the top differentially expressed marker genes were examined to determine their suitability for HCR. Genes that were particularly specific to the cluster of interest, had a very high level of expression as determined by the number of transcripts present, and where eight or more probe pairs could be designed were chosen for spatial analysis using HCR-FISH. The number of probe pairs was limited to 40 when necessary. DNA probe sets were designed using the Özpolat Lab probe generator (https://github.com/rwnull/insitu_probe_generator) [98]. The sequences generated by the algorithm were used to order DNA oPools™ Oligos from Integrated DNA Technologies (IDT), which were resuspended in nuclease-free H2O to a final concentration of 1 pmol/µL. All buffers and hairpin amplifiers were ordered from Molecular Instruments, Inc. The HCR-FISH protocol for *Hydractinia* was based on published methodology [99]. Adult feeding polyps dissected from the stolon mat and whole juvenile colonies were relaxed in 4% MgCl2 1:1 filtered seawater (FSW): H2O before being fixed in 4% paraformaldehyde (PFA) in 1x PBS + 0.1% Tween-20 (PTw) for 1–2 h at 4 °C. Samples were then dehydrated in increasing concentrations of methanol in PTw (25%, 50%, 75%, 100%) and stored at − 20 °C for at least 2 h. Following rehydration in a reverse methanol: PTw series (100%, 75%, 50%, 25%), samples were washed several times in PTw, before incubation in a solution of 50% PTw:50% probe hybridization buffer for 15 min at room temperature. Prehybridization was conducted for 1 h at 37 °C in 100% probe hybridization buffer. Following the one-hour prehybridization step, gene-specific probe sets were added to a final concentration of 20–40 nM, depending on the gene, and were generally hybridized for 16–24 h at 37 °C. For two genes (*HyS0045.75* and *HyS0053.57*), we found that the signal was improved by hybridization of probes for 6 days. After hybridization, prewarmed wash buffer was used to wash samples 4 × 15 min at 37 °C, followed by 3 × 5-minute washes with 5x SSCT (5x SSC, 0.1% Tween-20) at room temperature. Samples were then incubated in an amplification buffer for 30 min at room temperature. During this step, hairpins were prepared by adding 6 pmol of each hairpin (h1 and h2) into separate 0.5 mL tubes (the hairpin/fluorophore combination depended on the probe sets used) and heated to 95 °C for 90 s. Hairpins were then cooled to room temperature in the dark for 30 min. Finally, hairpin pairs were combined, and the appropriate volume of amplification buffer was added to create a 'hairpin solution' with a final volume of 100 µL. The pre-amplification solution was removed from samples and the appropriate 'hairpin solution' added to each tube. Samples were incubated overnight at room temperature in the dark. Samples were washed in 5x SSCT for 2 × 5 min, 2 × 30 min and finally 1 × 5 min. Hoechst 33,342 (ThermoFisher H1399) was included in one of the 30-minute wash steps at a final concentration of 10 µg/mL to stain nuclei. Finally, samples were mounted in 70% ultrapure glycerol: PBS before confocal

imaging. Negative controls were included for all hairpins used, where the procedure was followed as normal; however, probe sets were not added to the hybridization solution. Images of negative controls were captured using the same confocal settings used for experimental samples to ensure background fluorescence was not mimicking real signal. The complete list of probe sets and associated initiators for the 17 genes which were characterized using HCR-FISH (*HyS0042.111*, *HyS0008.263*, *HyS0032.220*, *HyS0020.22*, *HyS0056.60*, *HyS0002.425*, *HyS0027.82*, *HyS0013.338*, *HyS0049.55*, *HyS0004.446*, *HyS0041.99*, *HyS0078.51*, *HyS0048.57*, *HyS0001.363*, *HyS0016.300*, *HyS0045.75* and *HyS0053.57*) can be found in Supplementary Table S7.

HCR-FISH on dissociated cells

Approximately 40 adult feeding polyps were relaxed in 4% $MgCl_2$ 1:1 filtered seawater (FSW): H_2O for at least 15 min before being dissected from the stolon mat. Animals were decapitated and 'heads' and 'bodies' dissociated separately. Polyps were then washed two times in ACME solution in FSW (13:3:2:2 = FSW: methanol: acetic acid: glycerol), before being washed two times in ACME solution in diH_2O (13:3:2:2 = diH_2O: methanol: acetic acid: glycerol). Polyps were dissociated by vigorously pipetting solution up and down in 1 mL of ACME solution in diH_2O for several minutes. An ImmEdge® Hydrophobic Barrier PAP Pen was used to draw a circle on a SuperFrost slide (Cat. 12–550-15); 200 µL of dissociated cells were pipetted into the center of the circle and cells were left to settle overnight. HCR-FISH and Hoechst nuclei staining was performed on slides as above before imaging.

Fluorescent *in situ* hybridization (FISH)

Adult *Hydractinia* colonies were placed in a solution of 4% $MgCl_2$ in distilled water: filtered seawater (FSW) (1:1) for 10–15 min, before feeding polyps were cut from the stolon mat. Polyps were fixed for 90 s in an ice-cold solution of 0.2% glutaraldehyde, 4% paraformaldehyde (PFA) and 0.1%Tween-20 in FSW, followed by fixation in an ice-cold solution of 4% PFA and 0.1% Tween-20 in FSW for 90 min at 4 °C. Following fixation, samples were washed multiple times with ice-cold DEPC-PTw (1x phosphate-buffered saline (PBS) with 0.1% Tween20 in DEPC-treated H_2O) before being dehydrated with increasing concentrations of methanol in DEPC-PTw (25%, 50%, 75% and 100%). For two genes (*HyS0030.203* and *HyS0042.80*), Digoxigenin (DIG)-labeled riboprobes were generated with the SP6 or T7 MEGAscript kit (catalog #AM1334, #AM1330, Ambion, Inc., Austin, TX, USA) from cDNA clones (see Supplementary Table S7 for primer sequences used for PCR amplification and subsequent cloning of each gene). Immediately prior to *in situ* hybridization, samples were rehydrated with decreasing concentrations of methanol in DEPC-PTw, followed by several washes in DEPC-PTw. Samples were then washed for five minutes each in 1% triethylamine in DEPC-PTw (TEA), 0.6% acetic anhydride in TEA, and 1.2% acetic anhydride in TEA, followed by several washes in DEPC-PTw. Samples were pre-hybridized for 4 h at 55 °C in hybridization buffer (4 M urea, 0.1 mg/ml yeast tRNA, 0.05 mg/ml Heparin, 5x SCC pH7.0, 0.1% Tween20, 1% SDS in DEPC-treated H_2O). Riboprobes were diluted to a concentration of 0.5 ng/µL in hybridization buffer and heated to 90 °C for 10 min before being added to samples and incubated for approximately 40 h at 55 °C. Following hybridization, unbound probe was removed in a series of washes; hybridization buffer at 55 °C for 40 min and then decreasing hybridization buffer concentrations in 2x SSC at 55 °C, followed by washes with decreasing concentrations of 0.2x SSC in PTw at room temperature (RT). Endogenous peroxidase activity was quenched by two 30-minute washes in 3% hydrogen peroxide (H_2O_2), followed by further washes in PTw. Two 10-minute washes in maleic acid buffer (MAB, 100mM Maleic acid, 150mM NaCl, pH7.5) were then conducted. Samples were blocked for one hour in blocking buffer (Sigma-Aldrich, Cat. #11096176001 diluted 1:10 in MAB). Bound DIG-labeled riboprobe was detected by incubating samples overnight in 1:1500 dilution of Anti-DIG-POD antibody (Roche, Cat. # 11207733910) at 4 °C. Unbound antibody was removed by washing samples several times at room temperature in MABX (MAB containing 0.1% Triton X-100). Samples were then incubated in tyramide development solution (2% Dextran sulfate, 0.0015% hydrogen peroxide, 0.2 mg/ml Iodophenol, 1:100 Alexa Fluor 594 Tyramide Reagent (Thermo Scientific, Cat. # B40957) in PTw for eight minutes and then washed several times in PTw. Nuclei were stained using Hoechst dye 33342 (ThermoFisher, Cat. # H1399).

Microscopy and image analysis

All samples were imaged with a Zeiss LSM 710 confocal microscope (Zeiss, Gottingen, Germany), and Z-stack projections were generated using Fiji [100]. All figures were created in Adobe Photoshop (version 25.12.0) or Adobe Illustrator (version 29.1).

Supplementary Information

The online version contains supplementary material available at https://doi.org/10.1186/s12864-025-12201-9.

Supplementary Material 1.

Supplementary Material 2.

Acknowledgements

We would like to thank the following individuals for their assistance throughout the course of this study: Alice Young, Jim Thomas, Betty Barnabas, and many others at the NIH Intramural Sequencing Center (NISC) for scRNA-seq library construction, sequencing, advice, and support. We also thank Joe

Ryan for bioinformatic and computational support and advice, as well as the members of the Schnitzler lab for many thoughtful discussions and their support.

Authors' contributions
J.S., D.J., C.S., A.B. conceived and designed the study. J.S., D.J., J.W., C.S. contributed to the methodology, acquisition of data and analysis, and interpretation of data; J.S., D.J., J.W., A.B., C.S. wrote the main manuscript text or substantively revised it. J.S., D.J., C.S. contributed to the revisions. All authors reviewed the manuscript.

Funding
This work was supported by the National Institutes of Health (R35GM138156 to C.E.S.).
This research was also supported in part by the Intramural Research Program of the National Institutes of Health (ZIA HG000140 to A.D.B.). The contributions of the NIH author are considered Works of the United States Government. The findings and conclusions presented in this paper are those of the authors and do not necessarily reflect the views of the NIH or the U.S. Department of Health and Human Services.

Data availability
Raw sequence data for this study were deposited in NCBI under BioProject ID: PRJNA1263849 with SRA accession numbers: SRR33665854-SRR33665862. All scripts and processed data are available via GitHub: https://github.com/sjwu571/HyS_scRNAseq and Zenodo: https://doi.org/10.5281/zenodo.15151309. A single-cell browser is publicly available at https://sjwu571.shinyapps.io/hys-umap/ and can also be found at the ***Hydractinia*** Genome Project Portal https://research.nhgri.nih.gov/hydractinia/.

Declarations

Ethics approval and consent to participate
Not applicable.

Consent for publication
Not applicable.

Competing interests
The authors declare no competing interests.

Received: 18 July 2025 / Accepted: 8 October 2025
Published online: 11 December 2025

References

1. Weismann A. Die entstehung der sexualzellen Bei Hydromedusen (The origin of the sexual cells in hydromedusae). Jena: Gustav Fischer-; 1883.
2. Künzel T, Heiermann R, Frank U, Müller W, Tilmann W, Bause M, et al. Migration and differentiation potential of stem cells in the cnidarian *Hydractinia* analysed in eGFP-transgenic animals and chimeras. Dev Biol. 2010;348:120–9. https://doi.org/10.1016/j.ydbio.2010.08.017.
3. Frank U, Nicotra ML, Schnitzler CE. The colonial cnidarian hydractinia. EvoDevo. 2020;11:7. https://doi.org/10.1186/s13227-020-00151-0.
4. Müller W. Experimentelle untersuchungen über Stockentwicklung, polypendifferenzierung und Sexualchimären Bei hydractinia echinata. Wilhelm Roux' Archiv für Entwicklungsmechanik Der Organismen. 1964;155:181–268. https://doi.org/10.1007/BF00573905.
5. Müller W. Differenzierungspotenzen und Geschlechtsstabilität der I-Zellen von hydractinia echinata. W Roux' Archiv F Entwicklungsmechanik. 1967;159:412–32. https://doi.org/10.1007/BF00575613.
6. Plickert G, Kroiher M, Munck A. Cell proliferation and early differentiation during embryonic development and metamorphosis of *hydractinia echinata*. Development. 1988;103:795–803. https://doi.org/10.1242/dev.103.4.795.
7. Rebscher N, Volk C, Teo R, Plickert G. The germ plasm component Vasa allows tracing of the interstitial stem cells in the cnidarian *hydractinia echinata*. Dev Dyn. 2008;237:1736–45. https://doi.org/10.1002/dvdy.21562.
8. Plickert G, Frank U, Müller WA. *Hydractinia*, a pioneering model for stem cell biology and reprogramming somatic cells to pluripotency. Int J Dev Biol. 2012;56:519–34. https://doi.org/10.1387/ijdb.123502gp.
9. Bradshaw B, Thompson K, Frank U. Distinct mechanisms underlie oral vs aboral regeneration in the cnidarian *hydractinia echinata*. eLife. 2015;4:e05506. https://doi.org/10.7554/eLife.05506.
10. Waletich J, de Jong D, Schnitzler CE. Characterization of eight new hydractinia i-cell markers reveals underlying heterogeneity in the adult pluripotent stem cell population. 2024;2024.07.07.602406. https://doi.org/10.1101/2024.07.07.602406.
11. Macosko EZ, Basu A, Satija R, Nemesh J, Shekhar K, Goldman M, et al. Highly parallel genome-wide expression profiling of individual cells using nanoliter droplets. Cell. 2015;161:1202–14. https://doi.org/10.1016/j.cell.2015.05.002.
12. Sebé-Pedrós A, Saudemont B, Chomsky E, Plessier F, Mailhé M-P, Renno J, et al. Cnidarian cell type diversity and regulation revealed by Whole-Organism Single-Cell RNA-Seq. Cell. 2018;173:1520–e153420. https://doi.org/10.1016/j.cell.2018.05.019.
13. Siebert S, Farrell JA, Cazet JF, Abeykoon Y, Primack AS, Schnitzler CE, et al. Stem cell differentiation trajectories in hydra resolved at single-cell resolution. Science. 2019;365:eaav9314. https://doi.org/10.1126/science.aav9314.
14. Chari T, Weissbourd B, Gehring J, Ferraioli A, Leclère L, Herl M, et al. Whole-animal multiplexed single-cell RNA-seq reveals transcriptional shifts across *Clytia* medusa cell types. Sci Adv. 2021;7:eabh1683. https://doi.org/10.1126/sciadv.abh1683.
15. Levy S, Elek A, Grau-Bové X, Menéndez-Bravo S, Iglesias M, Tanay A, et al. A stony coral cell atlas illuminates the molecular and cellular basis of coral symbiosis, calcification, and immunity. Cell. 2021;184:2973–e298718. https://doi.org/10.1016/j.cell.2021.04.005.
16. Steger J, Cole AG, Denner A, Lebedeva T, Genikhovich G, Ries A, et al. Single-cell transcriptomics identifies conserved regulators of neuroglandular lineages. Cell Rep. 2022. https://doi.org/10.1016/j.celrep.2022.111370.
17. Hu M, Bai Y, Zheng X, Zheng Y. Coral–algal endosymbiosis characterized using RNAi and single-cell RNA-seq. Nat Microbiol. 2023;8:1240–51. https://doi.org/10.1038/s41564-023-01397-9.
18. Schnitzler CE, Chang ES, Waletich J, Quiroga-Artigas G, Wong WY, Nguyen A-D, et al. The genome of the colonial hydroid hydractinia reveals that their stem cells use a toolkit of evolutionarily shared genes with all animals. Genome Res. 2024;34:498–513. https://doi.org/10.1101/gr.278382.123.
19. Salamanca-Díaz DA, Horkan HR, García-Castro H, Emili E, Salinas-Saavedra M, Pérez-Posada A, et al. The hydractinia cell atlas reveals cellular and molecular principles of cnidarian coloniality. Nat Commun. 2025;16:2121. https://doi.org/10.1038/s41467-025-57168-z.
20. Sánchez-Carbonell M, Jiménez Peinado P, Bayer-Kaufmann C, Hennings J-C, Hofmann Y, Schmidt S, et al. Effect of methanol fixation on single-cell RNA sequencing of the murine dentate gyrus. Front Mol Neurosci. 2023. https://doi.org/10.3389/fnmol.2023.1223798.
21. Klompen AML, Sanders SM, Cartwright P. Venom system variation and the division of labor in the colonial hydrozoan *Hydractinia symbiolongicarpus*. Toxicon: X. 2022;14:100113. https://doi.org/10.1016/j.toxcx.2022.100113.
22. Thomas MB, Edwards NC, Cnidaria. Hydrozoa. In: Harrison FW, Westfall JA, editors. Microscopic anatomy of invertebrates. New York, NY: Wiley-Liss; 1991. pp. 91–183.
23. Tardent P. The cnidarian cnidocyte, a hightech cellular weaponry. Bioessays. 1995;17:351–62. https://doi.org/10.1002/bies.950170411.
24. Hwang JS, Takaku Y, Chapman J, Ikeo K, David CN, Gojobori T. Cilium evolution. Identification of a novel protein, Nematocilin, in the mechanosensory cilium of hydra nematocytes. Mol Biol Evol. 2008;25:2009–17. https://doi.org/10.1093/molbev/msn154.
25. Mills CE. *Podocoryne selena*, a new species of hydroid from the Gulf of Mexico, and a comparison with *hydractinia echinata*. Biol Bull. 1976;151:214–24. https://doi.org/10.2307/1540715.
26. Lange R, Plickert G, Müller WA. Histoincompatibility in a low invertebrate, *hydractinia echinata*: analysis of the mechanism of rejection. J Exp Zool. 1989;249:284–92. https://doi.org/10.1002/jez.1402490307.
27. Schuchert P. Observations on hydractinia aculeata (Hydrozoa, Cnidaria). Rev Suisse Zool. 2014;121:441–51.
28. Schnitzler CE, Song J, de Jong D. How single-cell transcriptomics of *Hydractinia* is informing the evolution of cnidarian sensory systems. Integr Comp Biol. 2025. https://doi.org/10.1093/icb/icaf090.
29. Cazet JF, Siebert S, Little HM, Bertemes P, Primack AS, Ladurner P, et al. A chromosome-scale epigenetic map of the hydra genome reveals conserved regulators of cell state. Genome Res. 2023;33:283–98. https://doi.org/10.1101/gr.277040.122.
30. Cole AG, Steger J, Hagauer J, Denner A, Ferrer Murguia P, Knabl P, et al. Updated single cell reference atlas for the starlet anemone nematostella vectensis. Front Zool. 2024;21:8. https://doi.org/10.1186/s12983-024-00529-z.

31. Stokes DR. Morphological substrates of conduction in the colonial hydroid hydractinia echinata. I. An ectodermal nerve net. J Exp Zool. 1974;190:19–45. https://doi.org/10.1002/jez.1401900103.
32. Pascale A, Amadio M, Quattrone A. Defining a neuron: neuronal ELAV proteins. Cell Mol Life Sci. 2008;65:128–40. https://doi.org/10.1007/s00018-007-7017-y.
33. Nakanishi N, Renfer E, Technau U, Rentzsch F. Nervous systems of the sea anemone *nematostella vectensis* are generated by ectoderm and endoderm and shaped by distinct mechanisms. Development. 2012;139:347–57. https://doi.org/10.1242/dev.071902.
34. Vijay-Kumar S, Kumar VD. Neurocalcin. In: Vogel HJ, editor. Calcium-Binding protein protocols: volume 1: reviews and case studies. Totowa, NJ: Humana; 2002. pp. 261–79. https://doi.org/10.1385/1-59259-183-3:261.
35. Hayakawa E, Fujisawa C, Fujisawa T. Involvement of hydra achaete–scute gene CnASH in the differentiation pathway of sensory neurons in the tentacles. Dev Genes Evol. 2004;214:486–92. https://doi.org/10.1007/s00427-004-0430-4.
36. Schmich J, Rudolf R, Trepel S, Leitz T. Immunohistochemical studies of GLWamides in cnidaria. Cell Tissue Res. 1998;294:169–77. https://doi.org/10.1007/s004410051167.
37. Chrysostomou E, Flici H, Gornik SG, Salinas-Saavedra M, Gahan JM, McMahon ET, et al. A cellular and molecular analysis of SoxB-driven neurogenesis in a cnidarian. eLife. 2022;11:e78793. https://doi.org/10.7554/eLife.78793.
38. Klimovich A, Rehm A, Wittlieb J, Herbst E-M, Benavente R, Bosch TCG. Non-senescent hydra tolerates severe disturbances in the nuclear lamina. Aging. 2018;10:951–72. https://doi.org/10.18632/aging.101440.
39. Leitz T, Morand K, Mann M. Metamorphosin A. a novel peptide controlling development of the lower metazoan *Hydractinia echinata* (Coelenterata, Hydrozoa). Dev Biol. 1994;163:440–6. https://doi.org/10.1006/dbio.1994.1160.
40. Grimmelikhuijzen CJP, Leviev I, Carstensen K. Peptides in the nervous systems of cnidarians: Structure, Function, and biosynthesis. In: Jeon KW, editor. International review of cytology. Academic; 1996. pp. 37–89. https://doi.org/10.1016/S0074-7696(08)61345-5.
41. Takeda N, Kon Y, Quiroga Artigas G, Lapébie P, Barreau C, Koizumi O, et al. Identification of jellyfish neuropeptides that act directly as oocyte maturation-inducing hormones. Development. 2018;145:dev156786. https://doi.org/10.1242/dev.156786.
42. Attenborough RMF, Hayward DC, Wiedemann U, Forêt S, Miller DJ, Ball EE. Expression of the neuropeptides RFamide and LWamide during development of the coral *Acropora Millepora* in relation to settlement and metamorphosis. Dev Biol. 2019;446:56–67. https://doi.org/10.1016/j.ydbio.2018.11.022.
43. Takahashi T. Comparative aspects of structure and function of cnidarian neuropeptides. Front Endocrinol. 2020. https://doi.org/10.3389/fendo.2020.00339. 11.
44. Weissbourd B, Momose T, Nair A, Kennedy A, Hunt B, Anderson DJ. A genetically tractable jellyfish model for systems and evolutionary neuroscience. Cell. 2021;184:5854–e586820. https://doi.org/10.1016/j.cell.2021.10.021.
45. Yamamoto W, Yuste R. Peptide-driven control of somersaulting in hydra vulgaris. Curr Biol. 2023;33:1893–905. https://doi.org/10.1016/j.cub.2023.03.047. .e4.
46. Hauser F, Koch TL, Grimmelikhuijzen CJP, Review. The evolution of peptidergic signaling in cnidaria and Placozoa, including a comparison with bilateria. Front Endocrinol. 2022;13. https://doi.org/10.3389/fendo.2022.973862.
47. Kon-Nanjo K, Kon T, Horkan HR, Febrimarsa, Steele RE, Cartwright P et al. Chromosome-level genome assembly of hydractinia symbiolongicarpus. G3 Genes|Genomes|Genetics. 2023;13:jkad107. https://doi.org/10.1093/g3journal/jkad107.
48. Grimmelikhuijzen CJP, Williamson M, Hansen GN. Neuropeptides in cnidarians. Can J Zool. 2002;80:1690–702. https://doi.org/10.1139/z02-137.
49. Prabhu P, Reddy PC. Identifying neuropeptides in hydra: a custom pipeline reveals a non-amidated regulator of muscle contraction and other new members. 2025;2025.03.12.642944. https://doi.org/10.1101/2025.03.12.642944.
50. Little HM, Primack AS, Tsverov J, Mühlbauer S, Cox BD, Busse C et al. A Molecular, Spatial, and regulatory atlas of the hydra vulgaris nervous system. 2025;2023.03.15.531610. https://doi.org/10.1101/2023.03.15.531610.
51. Rose PG, Burnett AL. An electron microscopic and histochemical study of the secretory cells in *hydra viridis*. Wilhelm Roux' Archiv für Entwicklungsmechanik der Organismen. 1968;161:281–97. https://doi.org/10.1007/BF00576681.
52. Haynes JF, Davis LE. The ultrastructure of the zymogen cells in *hydra viridis*. Z Zellforsch. 1969;100:316–24. https://doi.org/10.1007/BF00343886.
53. Augustin R, Franke A, Khalturin K, Kiko R, Siebert S, Hemmrich G, et al. Dickkopf related genes are components of the positional value gradient in hydra. Dev Biol. 2006;296:62–70. https://doi.org/10.1016/j.ydbio.2006.04.003.
54. Schwarz RS, Hodes-Villamar L, Fitzpatrick KA, Fain MG, Hughes AL, Cadavid LF. A gene family of putative immune recognition molecules in the hydroid hydractinia. Immunogenetics. 2007;59:233–46. https://doi.org/10.1007/s00251-006-0179-1.
55. Siebert S. Towards an Understanding of molecular mechanisms controlling gland cell behaviour in hydra. Doctoral dissertation, Christian-Albrechts Universität Kiel. 2008.
56. Bouillon J. Les cellules glandulaires des hydroïdes et hydroméduses. Leur structure et La nature de leurs sécrétions. Cah Biol Mar. 1966;7:157–205.
57. Buzgariu W, Al Haddad S, Tomczyk S, Wenger Y, Galliot B. Multi-functionality and plasticity characterize epithelial cells in hydra. Tissue Barriers. 2015;3:e1068908. https://doi.org/10.1080/21688370.2015.1068908.
58. Leclere L, Röttinger E. Diversity of cnidarian muscles: function, anatomy, development and regeneration. Front Cell Dev Biol. 2017;4. https://doi.org/10.3389/fcell.2016.00157.
59. Holstein TW. The *Hydra* stem cell system – revisited. Cells Dev. 2023;174:203846. https://doi.org/10.1016/j.cdev.2023.203846.
60. Weis V, Buss L. Ultrastructure of metamorphosis in *Hydractinia echinata*. Postilla. 1987;199:1-20.
61. Möhrlen F, Maniura M, Plickert G, Frohme M, Frank U. Evolution of astacin-like metalloproteases in animals and their function in development. Evol Dev. 2006;8:223–31. https://doi.org/10.1111/j.1525-142X.2006.00092.x.
62. Dandar-Roh AM, Rogers-Lowery CL, Zellmann E, Thomas MB. Ultrastructure of the calcium-sequestering gastrodermal cell in the hydroid hydractinia *Symbiolongicarpus* (Cnidaria, Hydrozoa). J Morphol. 2004;260:255–70. https://doi.org/10.1002/jmor.10220.
63. Sanders SM, Travert MK, Cartwright P. Frizzled3 expression and colony development in hydractiniid hydrozoans. Journal of Experimental Zoology Part B: Molecular and Developmental Evolution. 2020;334:311–7. https://doi.org/10.1002/jez.b.22980.
64. Lange RG, Müller WA, SIF. A novel morphogenetic inducer in hydrozoa. Dev Biol. 1991;147:121–32. https://doi.org/10.1016/S0012-1606(05)80012-0.
65. Zárate-Potes A, Ocampo ID, Cadavid LF. The putative immune recognition repertoire of the model cnidarian *Hydractinia Symbiolongicarpus* is large and diverse. Gene. 2019;684:104–17. https://doi.org/10.1016/j.gene.2018.10.068.
66. Mustelin T, Vang T, Bottini N. Protein tyrosine phosphatases and the immune response. Nat Rev Immunol. 2005;5:43–57. https://doi.org/10.1038/nri1530.
67. Dennis. Phospholipase A2 Enzymes: Physical Structure, Biological Function, Disease Implication, Chemical Inhibition, and Therapeutic Intervention | Chemical Reviews. https://pubs.acs.org/doi/full/10.1021/cr200085w. Accessed 9 May 2025.
68. Triggiani M, Granata F, Frattini A, Marone G. Activation of human inflammatory cells by secreted phospholipases A2. Biochimica et Biophysica Acta (BBA). 2006;1761:1289–300. https://doi.org/10.1016/j.bbalip.2006.07.003.
69. Cadavid LF. Self-discrimination in colonial invertebrates: genetic control of allorecognition in the hydroid *Hydractinia*. Dev Comp Immunol. 2004;28:871–9. https://doi.org/10.1016/j.dci.2004.01.007.
70. Nicotra ML, Powell AE, Rosengarten RD, Moreno M, Grimwood J, Lakkis FG, et al. A hypervariable invertebrate allodeterminant. Curr Biol. 2009;19:583–9. https://doi.org/10.1016/j.cub.2009.02.040.
71. Rosa SFP, Powell AE, Rosengarten RD, Nicotra ML, Moreno MA, Grimwood J, et al. *Hydractinia* allodeterminant *alr1* resides in an Immunoglobulin Superfamily-like gene complex. Curr Biol. 2010;20:1122–7. https://doi.org/10.1016/j.cub.2010.04.050.
72. Nicotra ML. The hydractinia allorecognition system. Immunogenetics. 2022;74:27–34. https://doi.org/10.1007/s00251-021-01233-6.
73. Bosch TCG, David CN. Immunocompetence in hydra: epithelial cells recognize self-nonself and react against it. J Exp Zool. 1986;238:225–34. https://doi.org/10.1002/jez.1402380212.
74. Olano CT, Bigger CH. Phagocytic activities of the Gorgonian coral *Swiftia exserta*. J Invertebr Pathol. 2000;76:176–84. https://doi.org/10.1006/jipa.2000.4974.
75. Mydlarz LD, Holthouse SF, Peters EC, Harvell CD. Cellular responses in sea fan corals: granular amoebocytes react to pathogen and climate stressors. PLoS ONE. 2008;3:e1811. https://doi.org/10.1371/journal.pone.0001811.
76. Parisi MG, Parrinello D, Stabili L, Cammarata M. Cnidarian immunity and the repertoire of defense mechanisms in anthozoans. Biology. 2020;9:283. https://doi.org/10.3390/biology9090283.

77. Snyder GA, Eliachar S, Connelly MT, Talice S, Hadad U, Gershoni-Yahalom O, et al. Functional characterization of Hexacorallia phagocytic cells. Front Immunol. 2021. https://doi.org/10.3389/fimmu.2021.662803.
78. Varley Á, Horkan HR, McMahon ET, Krasovec G, Frank U. Pluripotent, germ cell competent adult stem cells underlie cnidarian plant-like life history. 2022;2022.11.09.515637. https://doi.org/10.1101/2022.11.09.515637.
79. Quiroga-Artigas G, de Jong D, Schnitzler CE. GNL3 is an evolutionarily conserved stem cell gene influencing cell proliferation, animal growth and regeneration in the hydrozoan hydractinia. Open Biol. 2022;12:220120. https://doi.org/10.1098/rsob.220120.
80. Gupta S, Santoro R. Regulation and roles of the nucleolus in embryonic stem cells: from ribosome biogenesis to genome organization. Stem Cell Reports. 2020;15:1206–19. https://doi.org/10.1016/j.stemcr.2020.08.012.
81. David CN, Campbell RD. Cell cycle kinetics and development of hydra attenuata: I. epithelial cells. J Cell Sci. 1972;11:557–68. https://doi.org/10.1242/jcs.11.2.557.
82. David CN, Gierer A. Cell cycle kinetics and development of hydra attenuata: III. Nerve and nematocyte differentiation. J Cell Sci. 1974;16:359–75. https://doi.org/10.1242/jcs.16.2.359.
83. Bode HR, Heimfeld S, Chow MA, Huang LW. Gland cells arise by differentiation from interstitial cells in *Hydra attenuata*. Dev Biol. 1987;122:577–85. https://doi.org/10.1016/0012-1606(87)90321-6.
84. Fincher CT, Wurtzel O, de Hoog T, Kravarik KM, Reddien PW. Cell type transcriptome atlas for the planarian *Schmidtea mediterranea*. Science. 2018;360:eaaq1736. https://doi.org/10.1126/science.aaq1736.
85. Raz AA, Wurtzel O, Reddien PW. Planarian stem cells specify fate yet retain potency during the cell cycle. Cell Stem Cell. 2021;28:1307–e13225. https://doi.org/10.1016/j.stem.2021.03.021.
86. Rinkevich B, Ballarin L, Martinez P, Somorjai I, Ben-Hamo O, Borisenko I, et al. A pan-metazoan concept for adult stem cells: the wobbling Penrose landscape. Biol Rev. 2022;97:299–325. https://doi.org/10.1111/brv.12801.
87. García-Castro H, Kenny NJ, Iglesias M, Álvarez-Campos P, Mason V, Elek A, et al. Acme dissociation: a versatile cell fixation-dissociation method for single-cell transcriptomics. Genome Biol. 2021;22:89. https://doi.org/10.1186/s13059-021-02302-5.
88. Stuart T, Butler A, Hoffman P, Hafemeister C, Papalexi E, Mauck WM, et al. Comprehensive integration of Single-Cell data. Cell. 2019;177:1888–e190221. https://doi.org/10.1016/j.cell.2019.05.031.
89. Hao Y, Hao S, Andersen-Nissen E, Mauck WM, Zheng S, Butler A, et al. Integrated analysis of multimodal single-cell data. Cell. 2021;184:3573–e358729. https://doi.org/10.1016/j.cell.2021.04.048.
90. Choudhary S, Satija R. Comparison and evaluation of statistical error models for scRNA-seq. Genome Biol. 2022;23:27. https://doi.org/10.1186/s13059-021-02584-9.
91. McInnes L, Healy J, Saul N, Großberger L. UMAP: uniform manifold approximation and projection. J Open Source Softw. 2018;3:861. https://doi.org/10.21105/joss.00861.
92. Butler A, Hoffman P, Smibert P, Papalexi E, Satija R. Integrating single-cell transcriptomic data across different conditions, technologies, and species. Nat Biotechnol. 2018;36:411–20. https://doi.org/10.1038/nbt.4096.
93. Wickham H. Ggplot2: elegant graphics for data analysis. New York, NY: Springer-; 2016.
94. Gulati GS, Sikandar SS, Wesche DJ, Manjunath A, Bharadwaj A, Berger MJ, et al. Single-cell transcriptional diversity is a hallmark of developmental potential. Science. 2020;367:405–11. https://doi.org/10.1126/science.aax0249.
95. Cao J, Spielmann M, Qiu X, Huang X, Ibrahim DM, Hill AJ, et al. The single-cell transcriptional landscape of mammalian organogenesis. Nature. 2019;566:496–502. https://doi.org/10.1038/s41586-019-0969-x.
96. Alexa A, Rahnenfuhrer J, topGO: Enrichment Analysis for Gene Ontology. R package version 2.60.1. 2025. https://bioconductor.org/packages/release/bioc/html/topGO.html.
97. Teufel F, Almagro Armenteros JJ, Johansen AR, Gíslason MH, Pihl SI, Tsirigos KD, et al. Signalp 6.0 predicts all five types of signal peptides using protein language models. Nat Biotechnol. 2022;40:1023–5. https://doi.org/10.1038/s41587-021-01156-3.
98. Kuehn E, Clausen DS, Null RW, Metzger BM, Willis AD, Özpolat BD. Segment number threshold determines juvenile onset of germline cluster expansion in *platynereis dumerilii*. Journal of Experimental Zoology Part B: Molecular and Developmental Evolution. 2022;338:225–40. https://doi.org/10.1002/jez.b.23100.
99. Choi HMT, Schwarzkopf M, Fornace ME, Acharya A, Artavanis G, Stegmaier J, et al. Third-generation in situ hybridization chain reaction: multiplexed, quantitative, sensitive, versatile, robust. Development. 2018;145:dev165753. https://doi.org/10.1242/dev.165753.
100. Schindelin J, Arganda-Carreras I, Frise E, Kaynig V, Longair M, Pietzsch T, et al. Fiji: an open-source platform for biological-image analysis. Nat Methods. 2012;9:676–82. https://doi.org/10.1038/nmeth.2019.

Publisher's Note